Novel Rail Pads for Improved Noise Reduction and Reduced Track Maintenance

Final Report (Month 60, Draft Version)

Laboratory of Macromolecular and Organic Materials
Prof. Holger Frauenrath, Dr. Christopher J.G. Plummer

École Polytechnique Fédérale de Lausanne
EPFL–STI–IMX–LMOM, MXG 037, Station 12
1015 Lausanne, Switzerland

Laboratory for Processing of Advanced Composites
Prof. Véronique Michaud

École Polytechnique Fédérale de Lausanne
EPFL–STI–IMX–LPAC, MXH 147, Station 12
1015 Lausanne, Switzerland

Institute of Mechanical Design, Materials Science and Packaging Technologies (COMATEC), Prof. Joël Cugnoni

Haute École d'Ingénierie et de Gestion du Canton de Vaud
Route de Cheseaux 1
1401 Yverdon-les-Bains, Switzerland

Laboratory for Acoustics and Noise Control
Dr. Bart van Damme

Empa
Ueberlandstrasse 129
8600 Dübendorf, Switzerland

SBB Infrastructure
Dr. Jakob Oertli

SBB Infrastructure – Noise Abatement
Hilfikerstrasse 3
3000 Bern 65, Switzerland

Semperit Technische Produkte GmbH, Austria
Mr. Herwig Miessbacher

Semperit Technische Produkte GmbH
Triester Bundesstrasse 26,
2630 Wimpassing, Austria

Lausanne, 1st September 2022

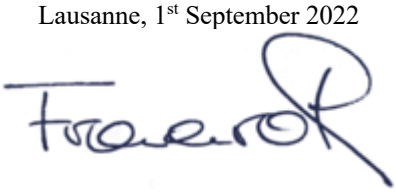

Prof. Holger Frauenrath (PI)

Summary

The main aim of the project *"Novel Rail Pads for Improved Noise Reduction and Reduced Track Maintenance"* was to take a rational, knowledge-based approach to optimizing rail pad performance with respect to standard reference SBB hard rail pads, while satisfying other operational requirements, based on the premise that high-damping rail pads should better dissipate vibrational energy on train pass-by. The specific design targets were: (i) rail-borne rolling noise reduction of 3–4 dB(A) with respect to soft rail pads and a noise reduction of at least 1 dB(A) with respect to the reference rail pads (sound power levels at a standard measurement point); (ii) stress distributions under the sleepers under low frequency cyclic loading consistent with an increase in ballast maintenance intervals by at least 10% with respect to the reference rail pads. To achieve these targets, we developed a modelling tool chain covering different length scales, from individual components to a full-scale, ballasted track, allowing experimental validation at each step. This was a key part of the design process and is relevant not only to rail pads but also to any component that contributes significantly to track dynamics and noise, so that its scope extends far beyond the immediate aims of the present project. The complete modelling tool chain will be available in a documented form suitable for autonomous use by qualified third parties equipped with the required software, and notably the open-source finite element analysis package, Code-Aster.

We used two basic modelling approaches, incorporating new, improved representations *in silico* of the rail pad and the ballast, taking into account their geometry and frequency dependent damping behaviour, based on input from extensive experimental measurements. In the first approach, a semi-analytical full track model was used for rapid coarse screening of rail pad materials, materials combinations, and 3D geometries with respect to rail noise and dynamic forces on the sleepers and ballast, and for parametric studies of the influence of rail pad stiffness and damping. The results from these latter provided a first demonstration of the effectiveness of rail pad damping in reducing rail noise, and an indication of the design space available for optimization. The second approach made use of full numerical simulations to give detailed and accurate predictions of the noise generated by the ensemble of the track under realistic loading conditions, and a complete 3D description of track displacements and loads over a wide range of frequencies. Our rail pad design strategy was based on a composite approach combining well characterized damping materials with elastic elements that allowed systematic tailoring of both stiffness and damping. This provided control over the local strain distribution for a given macroscopic solicitation, expanding the property envelope beyond that accessible to single material designs. Laboratory-scale prototypes were used to experimentally validate and refine the models, which were in turn used to assess improved designs. The most promising of these were finally retained for standard testing and eventual scale-up.

The main outcome of this process consisted of two working composite prototypes, and a single, high-damping material prototype suitable for scale-up within the time frame fixed by the field tests, produced by the industrial partner from a proprietary material, SemperSilent™, according to the project design specifications. The first composite prototype, based on a combination of the hard copolymer used in the reference rail pads, and a commercial high-damping rubber, was shown to give a 3 dB decrease in track noise under controlled excitation with respect to the reference rail pad, and was assigned a figure of merit for ballast protection, I_b, of 1.52 ($I_b = 1$ corresponds to the level of ballast protection provided by the reference SBB hard rail pads, and 1.10 is the minimum value consistent with a 10 % increase in ballast maintenance intervals). A reduction in track noise by as much as 4.5 dB and $I_b = 1.72$ were determined for the second composite prototype, based on a commercial hard polyester, Hytrel™ and SemperSilent™, while the corresponding values for the single material rail pad were 4.32 and 1.32, respectively.

These values, which were consistent with results from laboratory-scale tests, were considered to amply justify scale-up and the organization of full-scale field tests comprising train pass-by measurements. The field tests were carried out on a 100 m test section at Nottwil (LU) equipped with the single material SemperSilent™ rail pads, installed next to a similar track section equipped with the reference rail pads. Results from 101 individual pass-by events covering a variety of train and locomotive types showed the new rail pads to give a statistically significant reduction in the global noise levels, including not only rail noise, but also wheel and aerodynamic noise, by 0.73 dB(A), as well as significant reductions in vibration and the various frequency response functions associated with force transfer to the sleepers and ballast. In a next step, a concept will be developed by SBB to for the observation of the mid- to long-term behaviour of the new rail pads on a larger scale in several substantially longer track sections and to determine their cost-effectiveness, in terms of both acoustics and maintenance. This information will form the basis for decisions on the future use of the new rail pads. At the same, we see significant scope for further improvements in performance based on our results for the second Hytrel™/SemperSilent™ composite prototype, designed to be compatible with the industrial production processes used to produce the single material rail pads, but which offers the advantage of facile modulability while continuing to satisfy standard service requirements.

1 Introduction

This is an overview of work that started in September 2017 on the five-year project "Novel Rail Pads for Improved Noise Reduction and Reduced Track Maintenance", financed by the Swiss Federal Office for the Environment (*Bundesamt für Umwelt* (BAFU)). We first summarize the background and motivation for this project, its technical aims, hypotheses, methodology and structure (Sections 1.1–1.4). We then describe our main results and achievements (Section 2), assess these results in the light of our initial aims, and consider possible future developments (Section 3).

1.1 Background and Motivation

Noise pollution has greatly increased in recent years owing to demographic pressure, urbanization, and expanding transport infrastructure, with adverse consequences for life quality and health. The Swiss Confederation has long recognized reduced railway noise to be crucial to further improvements in the rail network, having enacted a first Noise Abatement Ordinance [1] in 1986 calling for limits on noise reception. This was followed by specific legislation in 2000 (*Bundesgesetz für die Lärmsanierung der Eisenbahnen*) and a 2001 ordinance (*Verordnung zur Lärmsanierung der Eisenbahnen*) that called for noise barriers, retrofitting of cast-iron braked vehicles with composite brake blocks, and insulated windows, a program that was completed in 2015. This legislation was subsequently revised to ban noisy freight wagons from Switzerland from 2020 and provide investment in the development of silent freight wagons. The revised legislation also included funding for research into and development of improved track damping and smooth rail surfaces.

Railway noise at typical train speeds in Switzerland is dominated by rolling noise [2]. In the four years up to the start of the present project, Swiss Federal Railways (SBB) therefore extensively tested different approaches to rolling noise mitigation and concluded additional elements such as rail dampers to be ineffective and lead to unacceptable additional costs due, e.g., to diagnostics or maintenance. As a result, SBB favours optimization of existing rail track components [3], and, in particular, the *rail pad* [4-6] an elastic cushion inserted between the rails and sleepers as part of the rail fastening system. Rail pads were introduced to prevent sleeper breakage due to replacement of wooden sleepers by more brittle concrete sleepers. They promote uniform loading at the rail-sleeper contact, and give the rails more freedom to bend under the weight of a passing train than if they are in direct contact with the sleepers, so that loads are more evenly distributed along the track. This reduces the maximum static or quasi-static loads (loads applied at rates where inertial effects may be ignored) on individual sleepers, and shields them from dynamic loads, which may exceed quasi-static loads if the local acceleration of the track components is high enough [7]. Recent deployment of “soft” rail pads has hence improved track superstructure protection by further diminishing transient loads and ground motion, allowing operators to increase ballast maintenance intervals and reduce costs, which are of increasing concern in Switzerland owing to intensification of railway traffic [3,8]. However, soft elastic rail pads also give the rails greater freedom to vibrate in response to excitation from train wheels, causing large increases in noise with respect to the reference hard rail pads currently used by SBB [2,3,9,10]. This is not only an inacceptable burden on the environment and populations near railway tracks but also incompatible with upcoming noise regulations. No working technical solution to this problem existed at the start of the present project, and none was foreseeable based on materials or components used in other countries.

1.2 Aims of the Project: Novel Rail Pads with Optimized Performance

1.2.1 Design Targets

The present project was set up to meet this challenge by developing new rail pads optimized with respect to noise and transient loads on the sleepers and ballast. The design targets were:

(i) A reduction in sound power levels[1] of 3–4 dB(A) compared with current soft rail pads, i.e., a reduction of at least 1 dB(A) with respect to the reference SBB hard rail pads.

(ii) A significant increase in track maintenance intervals and hence a decrease in track maintenance costs with respect to the reference SBB hard rail pads.

(iii) Compatibility with existing Swiss railway superstructure and cost-effectiveness.

[1] The sound power level generally used to quantify noise is defined as $10\log_{10} P/P_{ref}$ with units of dB or dB(A) if A-weighting is used to take into account the sensitivity of the human ear, where P is the sound power and P_{ref} is a reference power, usually taken to be 1 pW.

1.2.2 Initial Hypotheses

We initially postulated, and subsequently confirmed (Section 2), that our design targets could not be met with existing rail pad materials and would be difficult to meet with simple modifications to, or combinations of these materials. Our fundamental premise was that the performance of a rail pad may nevertheless be optimized by tailoring not only its mechanical stiffness and geometry, but also its viscoelastic properties, and hence its ability to damp acoustic vibrations. A strongly viscoelastic response implies rate-dependent hysteresis in the force-displacement response of the rail pad, allowing it to convert part of the mechanical energy associated with rail vibrations into thermal energy [10]. It should therefore in principle be possible to suppress noise in the critical frequency range 200–2'000 Hz where rail vibrations are the dominant source of noise, while reducing the rail pad stiffness, particularly at lower frequencies, which are of most concern for ballast settlement and track maintenance.

1.2.3 An Iterative Optimization Strategy: Design, Modelling, Experimental Verification and Feedback (Phase I)

There is growing interest in high-damping rail pads in the railway community, and it is known that frequency and strain dependent stiffness have a significant effect on track performance. However, rational optimization requires improved understanding of structure-property relationships in rail pads and their impact on track performance. The initial focus of the present project was therefore on obtaining comprehensive data for existing rail pads and rail pad materials, defining a rigorous technical framework for the new rail pads, and developing semi-analytical and numerical models that provide explicit links between rail pad geometry, materials properties, noise generation and superstructure protection. This is a complex hierarchical problem involving the ensemble of the rail track components, but its solution, and the consequent availability of validated models for rail track performance, has two major benefits. First, it allows one to establish limits on the noise reduction and superstructure protection that may be envisaged for rail pads with optimized stiffness and damping, and hence the feasibility of our approach. Second, it enables a systematic, iterative approach to design, based on materials combinations and geometries with potential for commercialization, without the need for costly, time-consuming homologation, scale-up, and field testing at each stage. Moreover, because such models incorporate detailed descriptions of the ensemble of the track components and their interactions, including the ballast, their potential applications extend well beyond the immediate requirements of the present project.

The first step in the modelling process was the experimental characterization of existing rail pad materials, rail pads and other track components. This allowed us to develop detailed rheological models for their behaviour that could be validated experimentally and incorporated into higher-level numerical and semi-analytical simulations. In the present case, we chose to carry out a combined experimental and modelling study of track dynamics and airborne noise generation based on a simple “three-sleeper cell”, suitable for experimental validation under well-controlled laboratory conditions. This provided a platform for the extension of both numerical and semi-analytical simulations to larger length scales and hence gain an idea of the merits of different rail pads in the field. However, it became clear that realistic treatments of the ballast than initially envisaged would be important to both refine full track models and better quantify the influence of rail pads on track degradation, taking into account the influence of under-sleeper pads (USPs), which are often used to smooth the load distribution at the sleeper-ballast interface. Indeed, a corollary of our modelling effort was that USPs may allow independent tailoring of the low and mid to high frequency track response, and hence contribute significantly to resolving the conflicting requirements for noise mitigation and superstructure protection.

1.2.4 Prototype Development (Phase II), Scale-up, and Field Testing (Phase III)

The validated simulations were used to develop design concepts for the optimization of rail pads with respect to noise and superstructure protection through control of their frequency-dependent stiffness and damping. The design and development strategy that emerged was initially based on combinations of a representative stiff material (ethylene vinyl acetate copolymer (EVA)), used in the reference SBB hard rail pads, and a material with strong damping in the frequency range of interest (modified polyisobutylene rubber (PIB)). These materials could be assembled virtually or experimentally at different length-scales and in different geometries to optimize the contribution of each component, resulting in reduced stiffness demonstrators that gave rail noise reductions of at least 1 dB(A) with respect to the reference rail pads in laboratory-scale tests, confirming the potential of our approach. This was the starting point for further development based on rapid feedback between materials properties, rail pad design, laboratory and large-scale testing, and modelling. An industrial partner joined the project at this stage to provide for scale-up of selected prototypes for final field testing. Because this also necessitated rigorous screening for safety reasons, normalized testing of the prototypes was initiated early in the project to leave time for adjustments. This included in-house testing and simulations aimed at screening prototype design iterations with respect to standard operational requirements.

1.3 Project Organization

The project was organized into the nine modules 1–9, comprising work packages to be attributed to specific project partners (Section 1.4). It was divided into the three separate phases, I, II, III (Table 1.1), already referred to in Section 1.2, with milestones that served as Stop/Go gates for the continued funding of the project by BAFU after Phases I and II.

Table 1.1. The three phases of the project "Novel Rail Pads for Improved Noise Reduction and Reduced Track Maintenance".

Phase I (Months 1–24). Detailed understanding of relationships between materials structure at the molecular, microstructural, and macrostructural length scales, the mechanical properties of rail pad materials and devices, and their impact on the acoustic and vibrational behaviour of the rail track.
Experimental testing of existing materials and devices (Module 1), review of existing solutions (Module 2), establishment of a rigorous technical framework for the new rail pads (Module 3), and development of a new modelling approach spanning the materials, sub-component, and systems levels (Module 4). The methodology adopted in Phase I was key to providing feedback on the effectiveness of novel rail pad materials and designs (Module 5), and the rational development of selected lead candidates in the subsequent phases of the project.
Phase II (Months 25–48). Development of the lead candidates from Phase I, ballast modelling, preparation for Phase III.
Further investigation of materials that show the desired frequency-dependent mechanical properties so as to enable development of new rail pad designs within the technical framework defined in Phase I (Module 6). Coordination between all project partners to ensure rapid feedback between materials development, rail pad design, mechanical testing, and modelling. Additional modelling and experimental work aimed at obtaining an improved understanding of ballast mechanics and the role of under sleeper pads (USPs). Integration of an industrial partner (rail pad manufacturer or materials transformer) with a view to scale-up for field testing (Modules 7 and 8).
Phase III (Months 49–60). Development of an industrially viable product with demonstrably improved performance in the field.
Scale-up of rail pad production, normalized laboratory testing for homologation, and performance evaluation of the new rail pads from pass-by measurements in real railway tracks (Module 8); final public dissemination of the results (Module 9).

1.4 Project Consortium

The multidisciplinary nature of the project and the need for a wide range of technical resources required multiple academic partners from different institutions around Switzerland (Table 1.2) covering materials science, the mechanics of dynamic systems, acoustics, modelling and control of environmental noise, and industrial liaison, together with representatives from SBB and an industrial partner responsible for scale-up of the final designs.

Table 1.2. Project partners and their affiliations.

Abbreviation	Institutions; Team Leaders
LMOM	Ecole Polytechnique Fédérale de Lausanne (EPFL), Laboratory of Macromolecular and Organic Materials; Holger Frauenrath, Christopher J.G. Plummer (Lausanne, VD)
LPAC	EPFL, Laboratory for Processing of Advanced Composites; Véronique Michaud (Lausanne, VD)
LMAF	EPFL, Laboratory of Applied Mechanics and Reliability Analysis; Joël Cugnoni (Phase I) (Lausanne, VD)
LTS2	EPFL, Signal Processing Laboratory; Hervé Lissek (Phase I) (Lausanne, VD)
TRACE	EPFL, Transport Centre; Simone Amorosi (Phase I) (Lausanne, VD)
HEIG	Haute École d'Ingénierie et de Gestion du Canton de Vaud (HEIG), Institute of Mechanical Design, Materials Science and Packaging Technologies (COMATEC); Joël Cugnoni (Phases II and III) (Yverdon-les-Bains, VD)
Empa	Empa, Laboratory for Acoustics and Noise Control; Armin Zemp, Bart van Damme (Dübendorf, ZH)
SBB	Swiss Federal railways (SBB) Infrastructure - Noise Abatement; Jakob Oertli (Bern, BE)
Semperit	Semperit Technische Produkte GmbH, Austria; Herwig Miessbacher (Phases II and III) (Wimpassing, Austria)

2 Main Results and Achievements

We begin by describing preparatory work carried out in Phase I aimed at establishing the technical requirements and feasibility of using high-damping rail pads to reduce rail noise in the light of previous work (Section 2.1). We then describe the experimental test methods (Section 2.2) and *in silico* modelling techniques (Section 2.3) on which our implementation of this concept in Phases II and III was based (Section 2.4), before considering the final prototypes selected for further development and scale-up for field tests (Section 2.5), and, finally, the results of the field tests (Section 2.6).

2.1 Framework Requirements, State of the Art, and Feasibility Studies

2.1.1 Technical Framework

The SBB technical framework and safety requirements, and project design targets were reassessed and defined in Phase I [11], focusing on use conditions, geometry, and mechanical properties. The new rail pads were required to be consistent with EN-13146, with a minimum area of 148 x 180 mm^2, an unloaded thickness of 7 mm, and a minimum stiffness of 200 kN/mm, and be suitable for use in continuously welded tracks, with 60E2 rails, B91 sleepers, the W14 fastening system, and USPs as an option. Other requirements included abrasion resistance, elasticity, resilience (shape recovery after deformation), longitudinal stiffness of about a third the vertical stiffness, stable geometry and properties, resistance to moisture, UV, ozone, hydrocarbons, and other railway-related chemicals, and a 20-year lifetime.

Guidelines were established for assessing the acoustic response of a rail track according to the standards, highlighting the importance of the balance between rail and sleeper noise and the effect of preloads due to the clamping system. Recommendations for management (track protection) included standards-based rail pad property measurements, track deflection measurements, and long-term monitoring of rail flats, other types of rail damage, static and dynamic rail pad stiffness, and the evolution of other critical track components. Specific test set-ups were also suggested for pass-by vibrations and the dynamic response of the rails and sleepers.

Two methods were considered for quantitative assessment of the trade-off between asset management, and suppression of noise and vibrations, namely cost-benefit and multi-criteria analysis. It was confirmed that improved asset management requires the new rail pads to be relatively soft, that noise should be reduced by at least 1 dB(A) compared with the current SBB hard rail pads, and that there should be no increase in vibration. Rail pads that meet these criteria may be significantly more expensive than the reference rail pads if their use is limited to noisy areas, but large cost increases are difficult to justify for rail pads intended for use throughout the rail network. However, rail pad development and the associated life-cycle costs involve complex interactions between multiple parameters, and flexibility should be maintained with regard to the technical framework. If an optimum design does not meet standard thickness requirements, for example, the additional costs involved in accommodating the non-standard thickness may still be justified for sufficiently large noise reductions.

2.1.2 Stakeholder Analysis

Key stakeholders were interviewed to assess their interest and influence, and potential opportunities for the project consortium [12]. The national regulation authority has the power to block implementation of new rail pads for reasons that may be hard to anticipate owing to the lack of a specific national process for rail pad approval in Switzerland, so that it is important to collaborate with this stakeholder in the early stages of development. The certification body may also delay implementation because of the need to involve a third party in the approval process, but in this case it is possible to choose from several accredited third parties. Support from citizen associations, e.g., in the form of political lobbying or communication via the mass-media, may be useful if another powerful stakeholder opposes implementation.

2.1.3 Assessment of Existing Rail Pad Materials and Solutions

A survey of scientific and patent literature on commercial rail pad materials and geometries, test methods and standards, current theoretical and modelling approaches, and polymers, polymer-based composites and fibrous or cellular materials with potential as rail pad materials, was submitted at the end of Phase I [13]. This provided a theoretical basis for subsequent work, with emphasis on materials with frequency-dependent stiffness and damping, and the uniqueness and feasibility of our proposed solutions.

It is well established (Section 1.1) that a rail pad should show low stiffness and reversible behaviour with respect to large static and low frequency transient loads in order to provide effective protection, but that any additional deformations

associated with vibrations that cause noise should also be suppressed. A prevalent strategy in industry is to increase the so-called “dynamic stiffness” (the stiffness at around 10 Hz as defined in the relevant standards) of the rail pad under service loads, so that rail vibrations are more strongly coupled to the sleepers and ballast once the rail has bent by a certain amount. Various other operating criteria related, e.g., to durability and abrasion resistance, and stability of the rail during train pass-by, are met for a broad range of polymers, providing designers with considerable scope to vary the static stiffness for a fixed rail pad geometry. Modification of the ratio of the dynamic stiffness to the static stiffness is then typically achieved using studs or ribs on the major faces of the rail pad, or controlled internal porosity.

Chemical, thermal, and mechanical characterization of existing rail pads confirmed that none of the polymers in widespread use shows strong damping at acoustic frequencies (20–20,000 Hz). Many other polymers do show damping peaks in this range at ambient temperature, and the position, strength and sharpness of the associated transitions may be adjusted by chemical modification, or the use of additives or suitable materials combinations. However, when used on their own, high-damping polymers may not provide sufficiently stable mechanical support and resilience, whence our interest in a composite approach for the optimization of the static and dynamic properties of a rail pad. The literature also emphasizes the complexity of the dependence of the track response on the rail pad [14-16,22,23]. Empirical approaches to design based on trial and error are hence unlikely to be efficient, underlining the need for new modelling tools for the design and virtual prototyping of rail pads, going beyond the state of the art, in which the rail pad is typically treated as a point element with frequency-independent properties.

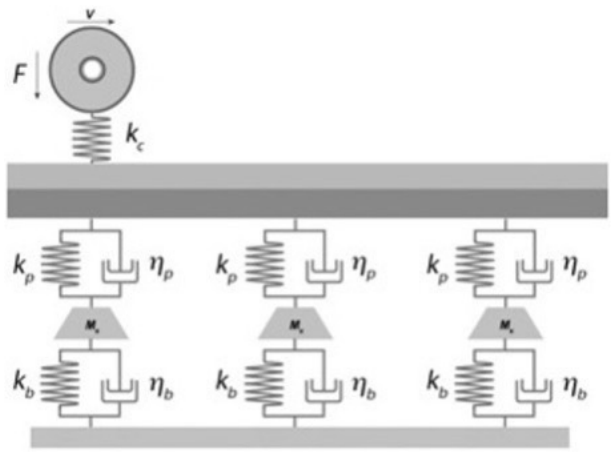

Figure 2.1. Analytical model for a track with a static or moving load. The rails are infinite beams mounted on either point-like or distributed massive supports representing the sleepers. The stiffness and damping of the rail pad and ballast are modelled using linear Kelvin elements, implying both to show linear viscoelastic behaviour, but these may be replaced by other arrangements, non-linear elements, or both, if required [14].

Even so, there has been a considerable effort to develop accurate simulations of the dynamic behaviour of a rail track incorporating 2D or 3D representations of the sleepers as either point-like or distributed supports with a well-defined spacing (usually 0.5 to 0.65 m) and position with respect to static or moving excitation sources [14,15]. Models based on finite elements (FE) or moving elements are the most versatile in terms of materials behaviour, geometry, and frequency range, but are computer-intensive, particularly at large track lengths [16]. Analytical models (Figure 2.1) offering more rapid turn-around, are therefore often preferred, but they incorporate simplifying assumptions about the response of individual components that limit their applicability [15]. However, for a reasonable choice of parameters, the resulting dynamic response, generally expressed as a frequency response function (FRF), defined in what follows as the acceleration corresponding to unit amplitude excitation force, shows common features with the response of real tracks in field measurements to excitation from an impact hammer or a shaker [14,17]. Of particular importance for noise is a rail resonance at about 1’000 Hz, called the “pin-pin” frequency, associated with bending of the rails with the sleepers at the nodes and a wavelength of twice the sleeper spacing [14].

A recurrent problem with both analytical and numerical models is that they typically incorporate simplified ballast representations, based, e.g., on linear Kelvin elements (cf. Figure 2.1). The real ballast response is non-linear, frequency dependent, and sensitive to the terrain the track crosses and its state of maintenance. It therefore varies considerably even among sleepers in a given track section [18]. Such effects are of particular concern for the low-frequency behaviour, which is also influenced by USPs [19-21]. Because excitation frequencies on train pass-by extend from 1 to over 3000 Hz, coupled rail and sleeper motion contributes significantly to rolling noise at low frequencies. However, the properties of the track support become less important for rail vibrations as the frequency increases in the range 500–2’000 Hz, to which the human ear is particularly sensitive, and in which the rails become progressively decoupled from the sleeper. Hence, while USPs may reduce ground vibrations by several dB, they have little effect on noise [24,25], as was confirmed in the present work by parametric studies using both semi-analytical and numerical track models (Section 2.3). Most current analytical models nevertheless fail to fully describe of the 3D dynamic response of the rails and sleepers, and improved numerical methods are needed to reproduce the more complex modes of vibration in real ballasted tracks.

The analytical approach is nevertheless useful for parametric studies of the influence of various track components on rolling noise at frequencies up to 2'000 Hz, beyond which sound is emitted mainly from the wheels [15]. It is known, e.g., that increased rail pad stiffness leads to increases in the cut-on frequency, i.e., the threshold for excitation of the first pin-pin mode, as well as reductions in the FRF at frequencies immediately below this frequency [14]. The intensity of the airborne pressure waves that give rise to rolling noise depends not only on the FRF, but also the length of the rail over which the vibrations persist. This excitation length is typically quantified in terms of the track decay rate (TDR) [dB/m], which is determined experimentally using accelerometers placed along the rails to measure the local vertical and horizontal frequency responses to an impact hammer [17]. The TDR is found to show a strong correlation with direct noise measurements on train pass-by in field tests, an increase in TDR by a factor two being reflected by a reduction in noise of about 3 dB at a given frequency [14,15]. Increased noise linked with soft rail pads may hence result from a decrease in both the cut-on frequency itself and the TDR above the cut-on frequency, where the FRF is relatively large.

The levels of sound emission due to track vibrations may also be quantified from analytical or numerical models for a suitable length of track [14,23]. The most complete simulations are based on FE models, which in principle give precise results for the full 3D sound pressure field at any frequency. However, it is also possible to estimate the sound pressure intensity at a given point in space analytically, given a suitable description of the dynamic response of the track to an excitation, by considering each element of the track surface to act as a point source. The results of such simulations generally reflect the observed inverse correlation between the TDR and sound emission [14].

2.1.4 Feasibility of Using High-Damping Rail Pads to Control Noise

An analytical model based on that of Thomson *et al.* [14] was used to establish the feasibility of noise control with high-damping rail pads, assuming frequency-independent stiffness and damping. This is inconsistent with classical viscoelasticity, which requires stiffness and damping to be frequency dependent (Section 2.3.1), but the limited frequency range over which rail noise is of most concern implies it to remain a useful basis for parametric studies. The model hence allowed us to quantify the effect of damping and establish if, and under which conditions damping may significantly reduce noise for a given rail pad stiffness. Each rail pad was characterized in terms of its "storage stiffness", k', which describes its elastic response to dynamic loads, and its "loss stiffness", k'', which describes the viscous contribution to the load, and hence the energy dissipation per cycle under dynamic loads. We may further define a "loss factor",

$$tan\,\delta = \frac{k''}{k'} \qquad (1),$$

which is a measure of a viscoelastic material's intrinsic damping capacity. $\tan\delta$ may reach as much as 2 in high-damping polymers but is generally below 0.2 in conventional rail pad materials. Finally, for the purposes of comparison, we define $\bar{p}$ to be the average sound pressure due to rail vibrations from 200 to 2'000 Hz determined at a measurement point equivalent to that used in field tests. Regardless of the details of the models (cf. Section 2.3.4), for a reasonable choice of track parameters and excitation force, we found a strong correlation between $\bar{p}$ and k' for a given $\tan\delta$ (Figure 2.2a). As $k' \longrightarrow 0$ the rails become fully decoupled from the sleepers, and hence free to vibrate, so that $\bar{p}$ tends to a relatively high plateau value, p_o, whereas in the limit $k' \longrightarrow \infty$, the rails and sleepers are strongly coupled and $\bar{p}$ tends to a second, lower plateau value, p_∞. The simulation results for constant $\tan\delta$ may then be approximated by a stretched exponential

$$\frac{\bar{p}}{p_\infty} = 1 + \left(\frac{p_o - p_\infty}{p_\infty}\right) exp\left[-\left(\frac{k'}{k_o}\right)^\alpha\right] \qquad (2),$$

where $\alpha \approx 0.45$ for $\tan\delta \gtrsim 0.2$ (Figure 2.3a) and k_o is a fitting parameter. Moreover, the k_o values obtained from fits of Equation 1 to the results for different $\tan\delta$ may be interpolated using

$$\frac{1}{k_o} \approx \frac{tan\,\delta}{k_a} + \frac{1}{k_b} \qquad (3),$$

where the fitting parameters k_a= 105 kN/mm and k_b= 1'400 kN/mm for the track parameters used here (Figure 2.2b). This implies that for strongly damping rail pads ($\tan\delta \gtrsim 0.2$)

$$\frac{\bar{p}}{p_\infty} \approx 1 + \left(\frac{p_o - p_\infty}{p_\infty}\right) exp\left[-\left(\frac{k''}{k_a}\right)^\alpha\right] \qquad (4),$$

i.e., that the rail noise depends only on k'' (Figure 2.3b). Although such simulations are not expected to reproduce the behaviour of a real track quantitatively without further refinement (cf. Section 2.3.4), they provide a first indication of the potential of high-damping rail pads, which to a first approximation may be modelled using predicted or experimental values of k' and $\tan\delta$ determined at 1,000 Hz, i.e., the mid-point of the frequency range over which $\bar{p}$ is defined.

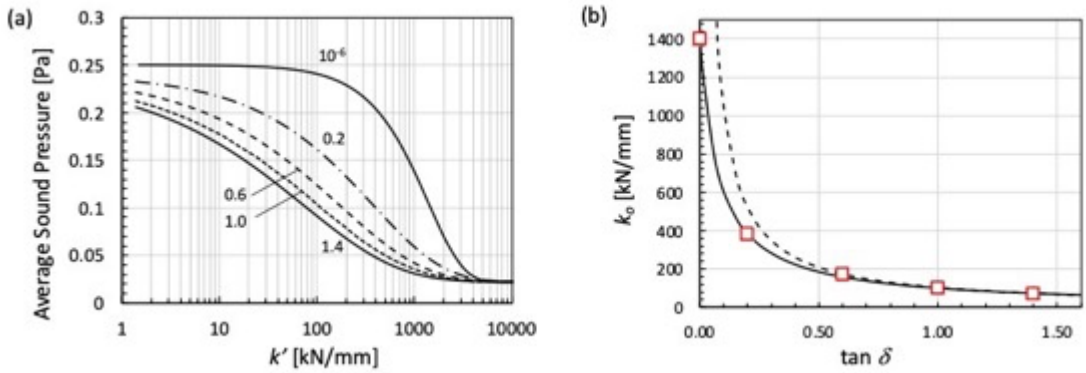

Figure 2.2. *a)* Semi-analytical simulations of the variation in average sound pressure due to rail vibrations at 200–2'000 Hz expressed as a function of k' for rail pads with different frequency independent $\tan\delta$ and a fixed vertical excitation force amplitude of 80 N applied midway between two sleepers. *b)* k_o from results for different $\tan\delta$ interpolated using Equation 3 (solid curve) or assuming $k_o = \tan\delta\,/k_a$ (hatched curve).

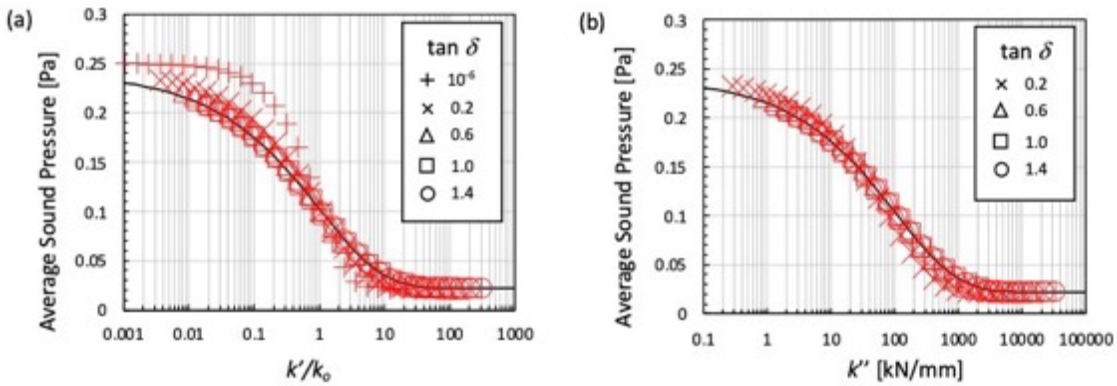

Figure 2.3. Simulated variation in average sound pressure generated by rail vibrations between 200 and 2'000 Hz: *a)* as a function of k'/k_o, where k_o is given by Equation 3 with k_a= 105 kN/mm and k_b= 1'400 kN/mm, for rail pads with different combinations of frequency independent k' and $\tan\delta$, compared with Equation 2 with $\alpha = 0.45$; *b)* as a function of k'' for $\tan\delta \geq 0.2$ compared with Equation 4, again with k_a= 105 kN/mm and $\alpha = 0.45$.

Figure 2.2 shows, e.g., that increasing k', results in a decrease in $\bar{p}$ for a given $\tan\delta$, consistent with the consensus that soft rail pads are nosier than hard rail pads (Section 1.1). To put this in the context of the design targets (Section 1.2.1), the difference between p_o and p_∞ in Equation 2, and hence the step height in Figure 1a, is equivalent to a difference in sound power of about 20 dB, which is far greater than the observed differences of around 3 dB between conventional low-damping hard ($k > 1'000$ kN/mm) and soft ($k < 100$ kN/mm) rail pads [14]. This is because only rail vibrations are considered here, whereas in practice there are significant contributions to noise from the wheels and sleepers [14]. Even so, noise variations in the frequency range of interest are dominated by the rails, so that it is significant that the model predicts reductions in $\bar{p}$ comparable with $p_o - p_\infty$ when $\tan\delta$ is increased for a wide range of constant k' values, confirming our initial hypothesis. However, there are limits to what may be achieved. There is little to be gained by, e.g., increasing $\tan\delta$ at very high k', because a very stiff rail pad will show little deformation and hence little damping, regardless of $\tan\delta$. It is only in regimes where $k'' \lesssim k_a$, where k_a is identified with the overall stiffness of the track, that a high-damping rail pad can take up a significant proportion of the deformation associated with rail vibrations, and hence dissipate significant amounts of energy. Damping is hence generally effective in reducing the average sound pressure for low to intermediate k', and Figure 2.2 confirms that it should be possible to reproduce the acoustic performance of a track equipped with hard rail pads by using softer rail pads with high $\tan\delta$. The challenge is then to maximize the tan δ of a rail pad while controlling its stiffness, which is non-trivial, because these quantities are interdependent in viscoelastic materials (Section 2.3.1). The implicit assumption here that softer rail pads provide better track superstructure protection may also need to be reconsidered for high-damping rail pads, because high $\tan\delta$ implies not only strong increases in elastic stiffness with increasing frequency, but also increased viscous forces.

2.2 Experimental Test Methods

2.2.1 Materials Mechanical Properties

Mechanical characterization of the various materials focused on small-strain dynamic mechanical analysis (DMA) in compression with various preloads designed to simulate loading conditions representative of the clamping system in a rail track, supplemented by measurements in tension and shear. Specimens were either prepared *ad hoc* or cut from as-received rail pads and the specimen dimensions were chosen according to the required stresses and the maximum range of the DMA load cell (5 mN to 40 N). Frequency sweeps over the approximate range 0.001–100 Hz were carried out at different temperatures, so that time-temperature superposition (TTS) could be used to extend the effective frequency range at a given temperature (Section 2.3.1). Large-strain tests to determine the onset of linearity and the yield stress made use of a screw-driven tensile test machine.

2.2.2 Track Component Testing

The stiffness of a rail pad is often significantly greater than implied by direct extrapolation of DMA results from small specimens because of confinement due to friction with the rail and the substrate and the planar geometry of the rail pad. There are hence significant contributions to stiffness from hydrostatic stresses, so that tests on the whole rail pad under conditions representative of a rail track are a key validation step for the simulations. Characterization of the non-linear response at high loads is also important for evaluating the quasi-static load redistribution between the sleepers under axle loading, which is in turn crucial for ballast protection. For this purpose, an MTS hydraulic test machine was used to apply vertical static or dynamic loads of up to 100 kN (representative of a passing train) at frequencies of up to 32 Hz to a single rail element clamped to the rail pad and a rigid substrate with the W14 fastening system. High-resolution sensors at four locations were used to measure displacements, and the loads and displacements were phase compensated for precise determination of $\tan\delta$. The MTS test machine was also used to determine single "static" and "dynamic" stiffnesses according to standard procedures, and for high-cycle fatigue testing using the same set-up, with rail pad stiffness and optical inspection as damage indicators. The fatigue test parameters were similar to those in the standard protocol (EN-13146), i.e., 3,000,000 loading cycles at 5 Hz with an amplitude of 86 kN, but only vertical loading was considered. Other components were subjected to vibration tests, e.g., measurements of the free vibration amplitudes in a suspended component induced by an impact hammer, used to validate the FE models (Section 2.3.5). Additional *ad hoc* tests introduced to support the ballast modelling effort are described in Section 2.3.3.

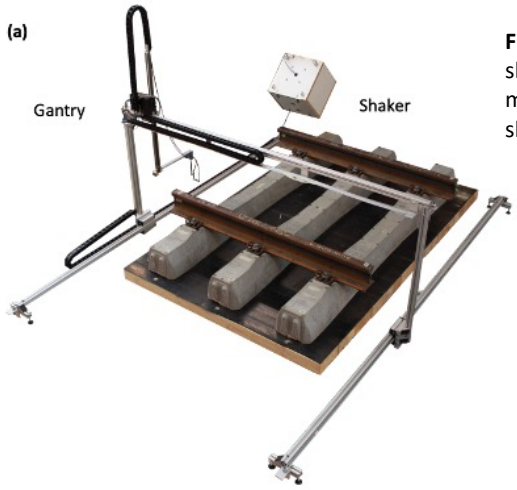

Figure 2.4. *a)* Installation of the three-sleeper cell at HEIG-VD, showing the shaker (top) and the gantry used for the acoustic measurements. *b,c)* 12-meter track test set-up used to investigate selected rail pads at TU Munich, showing *b)* the position of the measurement sensors and *c)* the shaker.

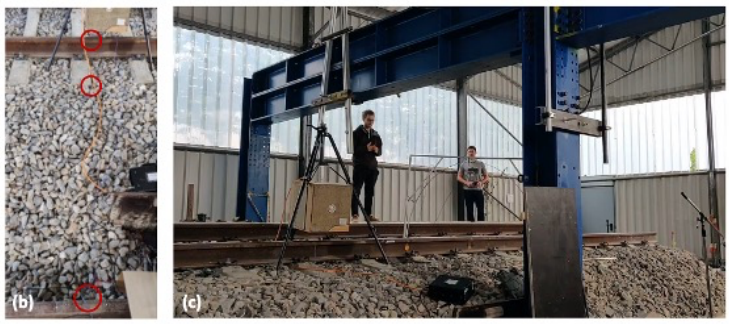

2.2.3 Three-Sleeper Cell

An instrumented three-sleeper rail track unit cell was set up in-house for the calibration and validation of FE models and as a test bed for repeatable, comparative assessment of rail pad prototypes. It comprised two 1.80 m rail segments, three B91 sleepers, six W14 clamps, six rail pads and a simulated ballast. This latter consisted of spruce beams aligned parallel to the rails with an intervening rubber layer to ensure uniform contact, providing similar elasticity to real ballast without the difficulties involved in ensuring reproducible properties from a granular support. An electromagnetic shaker or a monitored impactor was used to induce vibrations in the system, whose amplitudes were measured at each point of a predefined grid, giving access to the eigenfrequencies and mode shapes, and the FRF for each grid point. The acoustic measurement system made use of semi-automated gantry to displace a sound intensity probe around the unit cell (Figure

2.4a), and hence quantify the sound power radiated by the unit-cell on excitation by the shaker. This allowed steady background noise to be supressed, obviating the need for an anechoic environment while ensuring reliable, reproducible measurements.

2.2.4 Extended Track Section (TU Munich)

Selected rail pads were tested from the 30th of October to the 1st of September 2021 using a 12-meter rail-track section at TU Munich (*Technische Universität München*) for comparison with the simulation results and control measurements with the same set-up using the reference SBB hard rail pads, and to confirm scalability of both the numerical models and results from the three-sleeper cell. The track comprised 18 sleepers and a full ballast bed, and was excited using a shaker at its mid-point (Figure 2.4b). It was equipped with accelerometers, vibrometers, and seven microphones at and around the standard measurement position (10 cm spacing) for dynamic and acoustic characterization, giving access to various transfer functions and comprehensive noise measurements at seven different positions along the track.

2.2.5 Field Tests

Initial field tests for model validation took place between the 29th of November and the 1st of December 2018 on a track section near Winterthur (ZH) equipped with the reference SBB hard rail pads. Four types of measurement were made:

(i) FRF along the rail on excitation with an impact hammer following ES 15461 (vertical motion only).

(ii) FRF along the rail on excitation with a shaker (vertical and lateral motion) for the implementation of a new TDR calculation procedure.

(iii) FRF of a short rail segment on excitation with a shaker (vertical and lateral motion), allowing direct comparison with FE track models.

(iv) Sound levels and superstructure acceleration during pass-by events.

The standard TDR measurement method is based on wave attenuation, providing the imaginary part of the wavenumber k_I from fits of an exponential function to the vibration amplitude along the track at each frequency. However, for comparison with models it is also useful to access the real part of the wave number, k_R, because its measurement is typically more accurate. In the TDR calculation procedure introduced here, the inhomogeneous wave correlation (IWC) method was used to determine both k_R and k_I [26]. The measured or simulated track mobility was fitted with a damped wave $\exp(ik_R x - k_I x)$ at each frequency, where x is the distance along the rail, resulting in a full complex dispersion relation for the track. Experimental and simulated results for k_I were in good agreement with those from the standard method, while k_R showed a parabolic dependence on frequency, in accordance with the theory of bending waves.

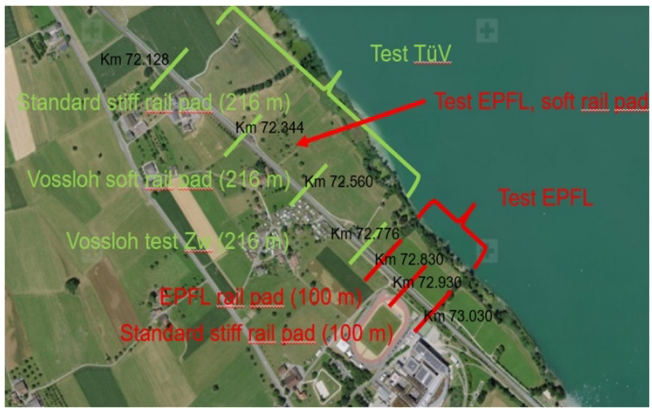

Figure 2.5. Field test set-up in Nottwil showing the two 100 m test sections with the new rail pads and the reference SBB hard rail pads. Soft rail pads were also available for comparison. The test sections used for the new rail pads are shown in red, while the sections used in previous tests are shown in green.

The final field tests on the prototype rail pads selected for upscaling in Phase III were carried out near Nottwil (LU), where SBB installed 100 m of the new rail pads between the 17th and 18th of March 2022 next to a 100 m section equipped with reference SBB hard rail pads in 2018 (Figure 2.5). The test section was easily accessible, and adjacent to a 200 m section equipped with soft rail pads (Vossloh, 60 kN/mm, 9 mm) for an earlier trial, also in 2018, allowing direct comparison with the new rail pads. All the track sections comprised 60E2 rails with steel quality R 260 rolled in 2018, B91 sleepers, the W14 fastening system, and stiff USPs (0.30 N/mm^3). The maximum speed on the track is 160 km/h and it has a yearly traffic of 42,868 passenger trains and 2,419 freight trains (data from 2019).

The noise and vibration measurements were carried out on the 16th–18th of March 2022, the 12th of April 2022, and the 16th of May 2022. They included pass-by microphone measurements according to ISO-3095, TDR and point mobility

measurements according to EN-15461, and vibration measurements of the rail and sleepers during pass-by. The measurement cross-sections were roughly at the mid-points of the "EPFL" parts of the track. The data were also included in the International Union of Railways (UIC) project LOWNOISEPAD involving 13 railway organizations, aimed at determining optimum specifications for rail pads in the different rail networks [27].

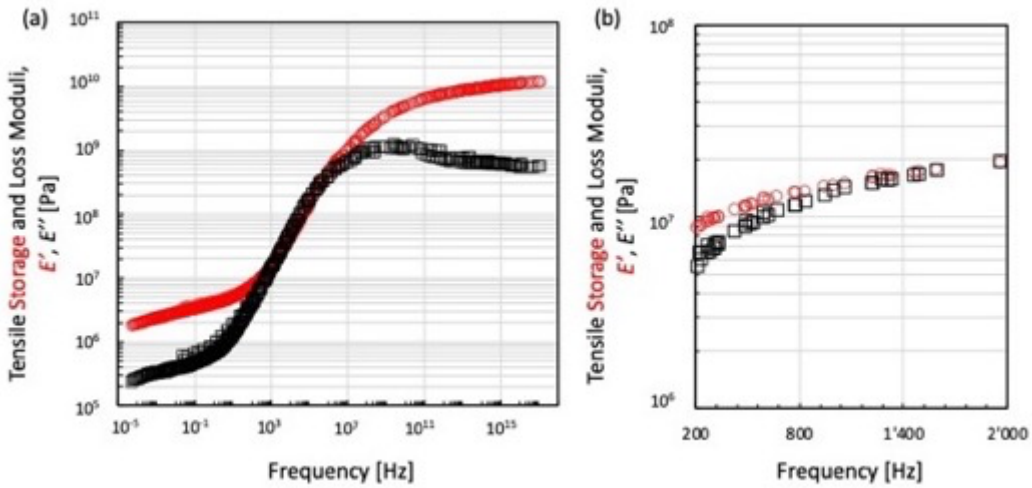

Figure 2.6. *a)* E' and E'' from tensile DMA data for the PIB initially used for demonstrator production in the present project obtained at different temperatures in the frequency range 0.01–100 Hz. The data were superposed using TTS to give a master curve corresponding to 21 °C. *b)* Detail in the frequency range 200–2'000 Hz.

2.3 Modelling Methods and Validation

2.3.1 Materials Modelling: Time Temperature Superposition (TTS), Parametrization of Dynamic Data

The dynamic viscoelastic response of a material may be described by a complex modulus, given by $E^* = E' + iE''$ in simple uniaxial tension or compression, where the storage and loss moduli, E' and E'', respectively, describe the in-phase (elastic) and quadrature (viscous) contributions to the tensile or compressive stress (load per unit area) for a periodic cyclic strain (deformation per unit undeformed length). In the absence of lateral constraints, E' and E'' are hence proportional to the dynamic stiffnesses, k' and k'' (Section 2.1.4), for a given geometry, and $\tan\delta = E''/E'$. In the linear regime, E' and E'' may be expressed as a function of frequency, f, using either a continuous relaxation time spectrum or a series expansion with an arbitrary number of adjustable constants, E_i, so that

$$E'[\omega] = E_\infty + \sum_{i=1}^{N} E_i \frac{(\omega\tau_i)^2}{1+(\omega\tau_i)^2}$$
$$E''[\omega] = \sum_{i=1}^{N} E_i \frac{\omega\tau_i}{1+(\omega\tau_i)^2} \quad (5),$$

where $\omega = 2\pi f$ is the angular frequency and τ_i are the relaxation times corresponding to each E_i [28,29].

It is a general feature of viscoelastic materials that raising the temperature, T, induces the same trends in physical properties as increasing the time available for relaxation or, equivalently, reducing ω at fixed T. If all the τ_i show the same dependence on T, and the E_i are proportional to T, assumptions that are physically justified for polymers that show a single dominant thermomechanical transition in the frequency range of interest, Equation 5 implies that

$$E'[a_T\omega,\, T_R] = \frac{\rho[T_R]T_R}{\rho[T]T} E'[\omega,\, T] \approx E'[\omega,\, T] \quad (6),$$

where ρ is the density, T_R is a reference temperature and a_T is a T-dependent shift factor such that $\tau_i[T] = \tau_i[T_R]a_T$. This is the basis for using TTS to construct a master curve for the frequency dependence of the viscoelastic functions (e.g., E', E'' or $\tan\delta$) at T_R that covers a far wider range of frequencies than are accessible to conventional experimental techniques [28,29]. Data for the viscoelastic functions plotted against $\log_{10}\omega$ for different T are corrected for ρ and the linear dependence of the E_i on T and then translated along the $\log_{10}\omega$ axis so that they overlap with the data obtained at T_R (Figure 2.6). The magnitude of the translation in each case is $\log_{10} a_T$.

In the present work, the fractional Zener model [30] was preferred to Equation 5 when fitting data analytically, because it offered good accuracy with only four fitting parameters. These could be determined automatically where limiting values of E' at the extremes of the frequency, and a clear peak in $\tan\delta$ could be identified unambiguously from TTS master curves. For materials with multiple thermomechanical transitions, or melting behaviour rather than elasticity at low frequencies, selection of an appropriate temperature range for the procedure was crucial. It was therefore important to confirm the accuracy of the analytical fits by careful comparison with the experimental data, and extend the models using more complex analytical formulations, if necessary. To account for non-linear effects, fits were made to data for different preloads and the results interpolated to give a full description of the behaviour in the load-frequency domain. This could then be used together with the bulk (hydrostatic compression) modulus, K, typically assumed to change little over large ranges of temperature and frequency, to construct FE models for the complete rail pads.

2.3.2 Rail Pad Models: FE Simulations, Super-elements, Simulation of Standard Tests

The commercial Dassault Simulia Abaqus™ FE solver initially used to implement FE models for the rail pads, was later replaced by Code-Aster, an open-source solver available at https://www.code-aster.org, and the stiffnesses and $\tan\delta$ predicted by the two solvers for standard geometries and hard or soft materials (EVA or PIB) were consistent. Provision was made not only for complex geometries but also for different materials combinations. Where this involved microstructural features such as porosity or fillers, a random microstructure generator was set up with the Mathworks Matlab™ software package and a mesh generated with the in-house "VoxelMesher" code for use with the FE solver. The viscoelastic properties in the frequency domain were then evaluated from harmonic simulations with an applied cyclic strain by monitoring the internal stresses.

Obtaining an accurate 3D representation of the behaviour of a given rail pad over a wide frequency range was nevertheless far from trivial, particularly for soft materials such as PIB, whose behaviour is highly sensitive to geometrical constraints in the absence of porosity, and hence to K, which is difficult to determine experimentally with sufficient precision. This was compounded by the need to assume idealized interfacial interactions, so that, e.g., slip between the rail pads and substrates at large deformations was not taken into account. It was therefore often necessary to adjust the constitutive equations empirically to obtain satisfactory agreement with the experimental data. Indeed, the need to offset the observed stiffening effect of 3D constraints on soft monolithic rail pads motivated our use of compressible inclusions, cavities, and surface grooves in the prototype designs. However, we generally obtained good agreement between the simulated and measured stiffness and damping (Table 2.1) in the frequency range directly accessible to the MTS (Section 2.2.2), justifying the use of the simulations to model rail pad properties over a wider frequency range.

Table 2.1. Comparison of properties predicted from FE simulations (where available) and properties measured in the frequency range directly accessible using the MTS for the principal rail pads investigated.

			10 Hz				20 Hz			
	k [kN/mm]		k' [kN/mm]		$\tan\delta$		k' [kN/m]		$\tan\delta$	
	Exp	*Sim*	Exp	*Sim*	Exp	*Sim*	Exp	*Sim*	Exp	*Sim*
SBB Hard	1,407	1,358	2,112	2,964	0.09	0.15	2,231	3,108	0.11	0.15
SBB Soft	354	277	479	606	0.09	0.15	636	635	0.11	0.15
PIB	382	468	722	835	021	0.30	863	922	0.29	0.36
SemperSilent™ 9 mm	165	160	281	204	0.27	0.27	340	222	0.31	0.26
PU Soft	33	29	40	46	0.09	0.06	41	47	0.09	0.06
D-groove EVA/PIB	292	–	526	–	0.17	–	–	–	0.23	–
4-groove EVA/PIB	477	425	957	805	0.24	0.26	1,116	878	0.33	0.30
Opt 4-groove EVA/PIB	527	460	861	895	0.2	0.24	927	969	0.25	0.27
SemperSilent™ 7 mm	244	238	454	304	0.31	0.27	561	331	0.40	0.26
Hytrel/ SemperSilent™	334	–	581	–	0.16	–	654	–	0.25	–

FE models were also developed to simulate loading cases corresponding to the various standards for rail pad and clamping system certification. This was particularly important for fatigue measurements according to EN-13146 (Section 2.5.1)

which involved application of application of a cyclic load of amplitude 83 kN at 33 ° to the vertical. As long as the maximum local von Mises stresses calculated from the simulations were well below the quasi-static threshold for yielding (about 20 MPa for EVA), creep was assumed to be negligible. This approach was used iteratively to optimize designs with respect to certification, and in the case of EVA/PIB composite rail pads, the results could be benchmarked with a standard reference SBB soft rail pad, also made from EVA, but strongly profiled, leading to higher stresses than in the hard rail pad.

Despite their usefulness, the FE models for the rail pads contained thousands of degrees of freedom (DoFs) and hence required considerable computational resources, particularly for systems-level simulations involving large numbers of rail pads (cf. Section 2.3.5). A Craig-Bampton technique (CMS) based on modal analysis and was therefore used to reduce the FE model to a super-element (SE), able to account for the rail pad geometry and materials properties with only 12 DoFs corresponding to the translations and rotations of the rail pad interface. A limitation of classical CMS is that viscoelasticity cannot be directly included. To overcome this, a multi-modal approach [31] was used to extract frequency-dependent complex stiffnesses, which could then be used to represent the rail pads in the semi-analytical models (2.3.4).

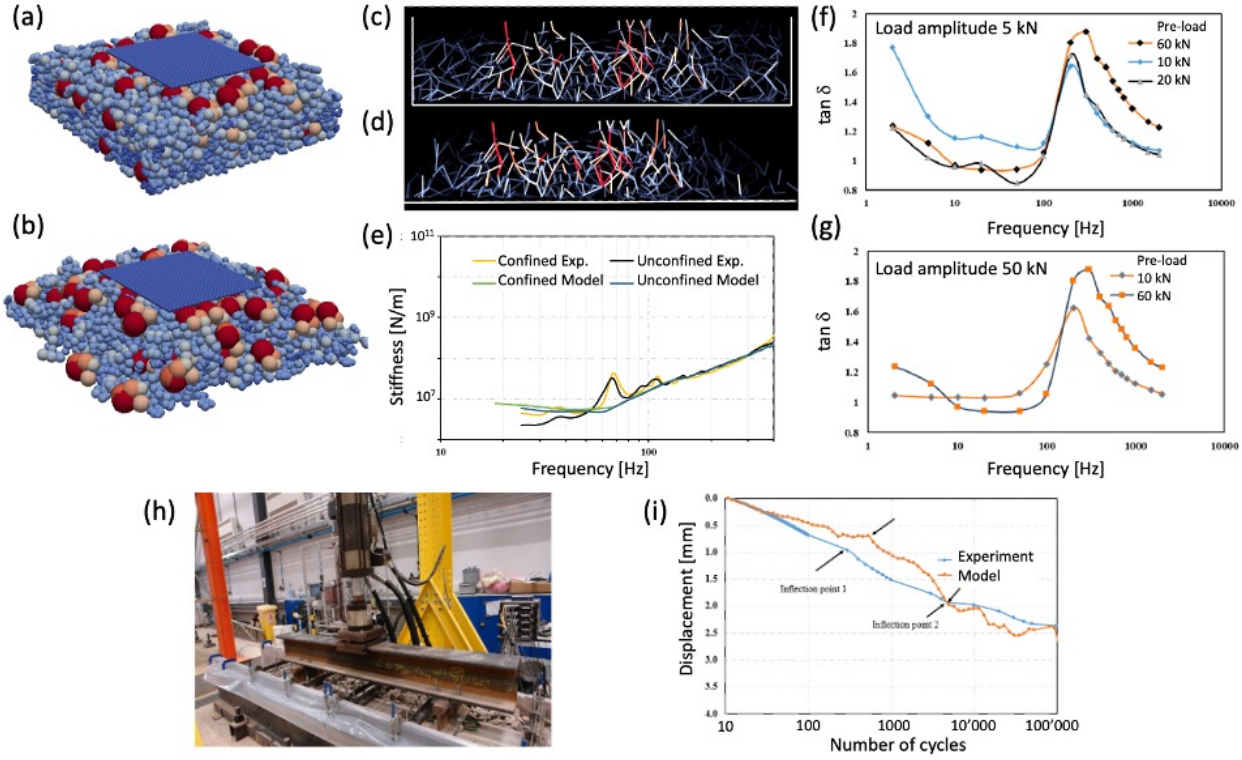

Figure 2.7. DEM for *a)* confined and *b)* unconfined ballast. Force network in the *c) c)* confined and *d)* unconfined ballast. *e)* Comparison of the experimental and calculated dynamic stiffnesses as a function of frequency in the confined and unconfined cases. *f,g)* Calculated damping factors for different preloads and cyclic force amplitudes. *h)* Image of the test facility at the University of Southampton used for the sedimentation measurements. *i)* Comparison of the predicted and experimental sedimentation results for ballast representative of that used in Switzerland.

2.3.3 Ballast Models

A discrete element model (DEM) [32] was developed in Phase II to provide more realistic representations of ballast dynamics in the track models, taking into account preload and frequency, and better understand the effect of long-term cyclic loads on settlement, with implications for track protection. The DEM treats ballast interactions at the particle level by counting the contacts between a granule and its neighbours, and calculating the reaction forces and displacements associated with these contacts for all the granules in the model. It hence provides insight into force propagation, stress concentrations, and individual ballast particle motion, that is difficult to access experimentally.

The DEM was first benchmarked using spherical steel shot. Ballast particles were then modelled as rigid “clumps” of up to five spheres, whose contact parameters and properties were optimized with respect to experimental data from confined ballast representative of that used by SBB, loaded under impact conditions via a rigid instrumented steel plate (Figure 2.7a). The optimized DEM was then subjected to cyclic loads with a pre-compression of 10–100 kN at frequencies of 10–2,500 Hz until a steady state was reached, and the results validated from the corresponding experimental data (Figure 2.7f,g). The homogenized frequency-dependent stiffness and damping of the ballast could then be extracted from

the resulting force-displacement curves for use in rail track models (Figure 2.7e). Subsequent DEM simulations of impact on unconfined ballast (Figure 2.7b) showed confinement to have a minimal effect on the dynamic stiffness, as reflected by the force network (Figure 2.7c,d), which was limited to regions of the ballast immediately below the loading plate. This opened the way to more realistic simulations incorporating a sleeper and an extended, partially confined ballast bed. Ballast settlement rates were investigated using the same methods, but with large-amplitude cyclic loads. The results were validated from experimental measurements carried out at a specialized measurement facility in the University of Southampton, again using ballast representative of that used by SBB (Figure 2.7h,i), and applying up to 4 million cycles at 4 Hz with an amplitude of 45 kN.

2.3.4 Improved Semi-Analytical Full Track Model

An improved semi-analytical model was developed for rapid screening, in which the rail head, web and foot, represented by Timoshenko beams, were placed on a discrete support consisting of 200 sleepers, also represented by Timoshenko beams, and the ballast, represented by a continuous viscoelastic layer. In contrast to previous models, the rail pad geometry and frequency dependent properties were incorporated via an SE (Section 2.3.2). This allowed the dynamics of the system to be simulated over an extended frequency range, providing output such as the rail deflection, speed, and acceleration, from which the TDR and sound pressure due to rail vibrations could be determined, as well as sleeper displacements. USPs were represented in the model using an equivalent complex stiffness in place of the ballast stiffness.

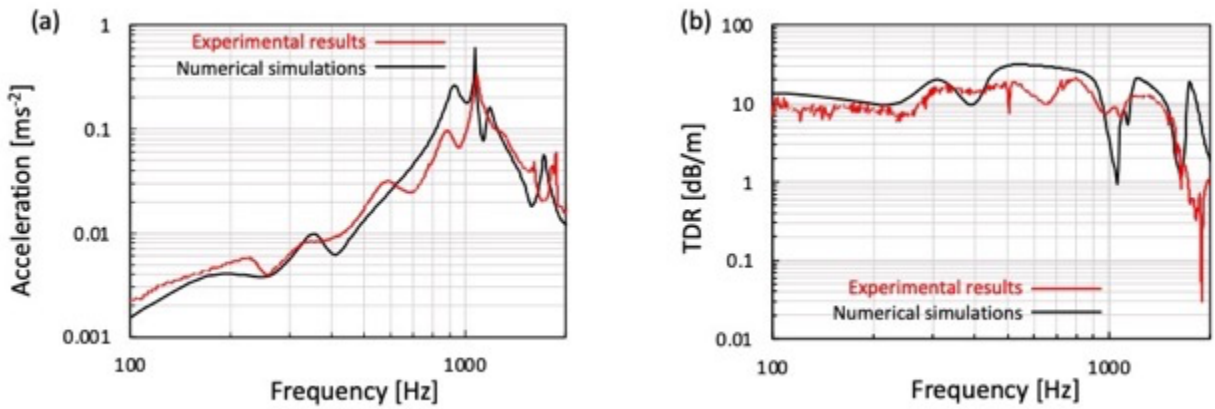

Figure 2.8. Comparison of results of the semi-analytical complete railway model with field test results from a railway track near Winterthur, Switzerland: *a)* acceleration, *b)* TDR.

With suitably tuned input parameters, e.g., those describing the ballast response, which were updated as input from DEM became available (Section 2.3.3), the semi-analytical model provided satisfactory simulations of the results from the Phase I field tests (Section 2.2.5). Because the simulations did not take into account train speed and quasi-static loading of the track system during a pass-by event, validation was based on impact hammer measurements, which were used to determine track accelerations and the TDR according to EN-15461. The model accelerations were in good quantitative agreement with the observed accelerations and most of the resonances were reproduced (Figure 2.8a), with the exception of a minor resonance at around 680 Hz seen in both track locations used for the measurements. Similarly good agreement was obtained with the TDR (Figure 2.8b). However, while the cut-off frequency immediately above 1,000 Hz was correctly estimated, the simulated peak at about 1,800 Hz was absent from the measured TDR, suggesting anomalous damping or absorption. It should be emphasized that the semi-analytical model was not intended as an alternative to the FE simulations, which provided a far more detailed representation of both the rail pad and the rail track, and simulated noise from the ensemble of the track components. However, it allowed for rapid preliminary assessment of different rail pad designs, as well as systematic parametric studies (cf. Section 2.1.4).

2.3.5 FE-Based Numerical Track Models: Three-Sleeper Cell, Extension to Larger Numbers of Sleepers

3D simulations of the laboratory-scale three-sleeper unit cell (Section 2.2.3) were again initially implemented in Abaqus™ but later transferred to Code-Aster. The FE model for the unit cell allowed harmonic simulation of the FRF at several points along the rails for a harmonic excitation force at a fixed location and was validated with data from the experimental set-up (Figure 2.9). Acoustic pressures were estimated by taking each surface element of the three-sleeper model to be a monopole acoustic source, again leading to good agreement with experimental data (Figure 2.10). To privilege rail vibrations, and provide insight into the global response of the set-up, a rail load of 45 °, representative of curved track

sections, was adopted for comparative studies. However, this was later adapted in the light of pass-by data from Winterthur (Section 2.2.5), to give a lateral rail load that was 10 % of the vertical load, equivalent to a 5.7 ° tilt of the shaker from the vertical, considered to be more representative of straight track sections.

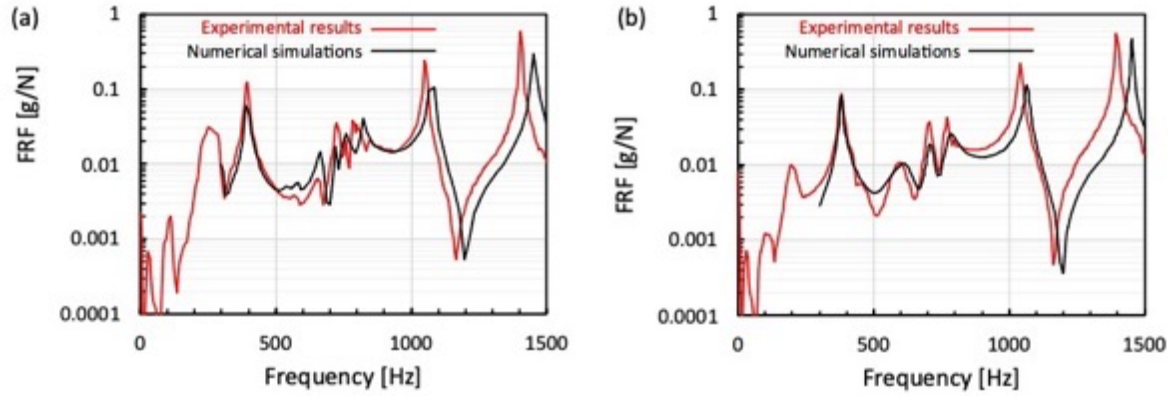

Figure 2.9. Comparison of results from simulations based on experimental constitutive models and data for the frequency response of the three-sleeper cell with 45 ° loading: *a)* reference SBB hard rail pads and *b)* monolithic PIB rail pads.

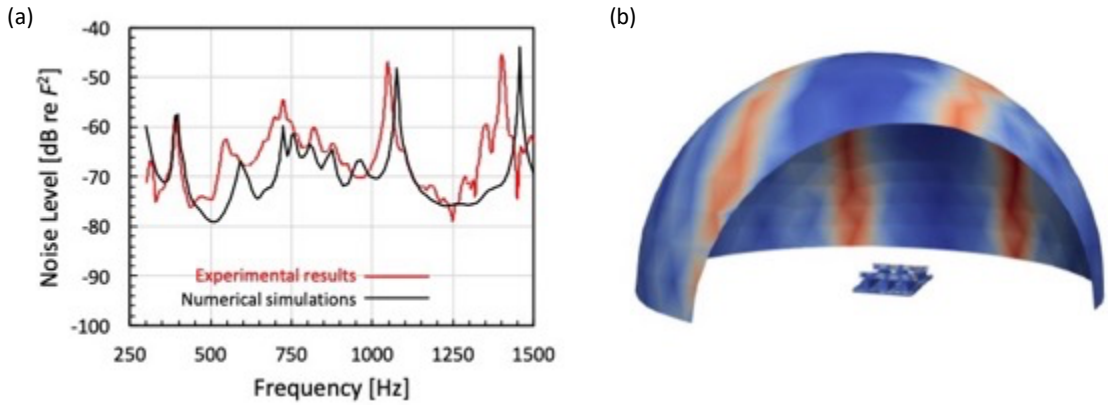

Figure 2.10. *a)* Comparison of results from simulations based on experimental constitutive models and experimental results for the normalized sound power from the three-sleeper cell with 45 ° loading and the reference SBB hard rail pads, defined as $L_w = 10\log_{10}(P/F^2)$ [dB] where P is the sound power and F is the shaker input force amplitude. The results of a numerical simulation are shown schematically in *b)*, the colours representing the sound pressure on a 3D half-shell surround the three-sleeper unit cell. *c)* Comparison of the simulated (blue) and experimental (orange) normalized logarithmic aggregate sound power levels in the range 300–1,500 Hz for an excitation angle of 45 ° for the various rail pads indicated.

The response of the track to loading from a passing train was assessed from quasi-static simulations using the three-sleeper cell. The stress in the ballast under the sleeper could then be used to predict the ballast settlement rate (Section 2.4.3), based, e.g., on literature models, or the ballast settlement models developed in the present project (Section 2.3.3). The same simulations were also used to verify that the rail pads showed sufficient resilience under fatigue loading conditions associated with successive impacts by multiple bogies, and that their vertical and horizontal deformations were low enough to ensure adequate rail stability. Typical results from simulation of loading and recovery on pass-by of five wagons showed that while short-term recovery was delayed by viscoelasticity, the residual strains were very small compared with the maximum strains after a time interval corresponding to successive bogies moving at 100 km/h. This was verified for all the rail pad designs under consideration so that lack of resilience was not considered to be a problem, at least under limited fatigue loading.

A full-scale FE rail track model was derived by extending the three-sleeper model to an arbitrary number of sleepers, and coupling it to a full-scale acoustic simulation model, the Oberbau-Simulations-Tool (OST), previously developed and validated at Empa [33]. This model was successfully validated from field measurements carried out on a track section near Winterthur equipped with standard hard EVA rail pads. However, because the original model was extremely computer intensive, requiring days for a single full track simulation, a new multi-sleeper model was introduced, based on dynamic sub-structuring, allowing vibro-acoustic simulation of an extended section of rail track at low computational cost (30 min to calculate the full spectrum dynamic response).

The updated model was validated with respect to the three-sleeper unit-cell, and then used to simulate to an 18-sleeper track section, using a more realistic representation of the ballast based on discrete spring-dashpot elements derived from the DEM studies (Section 2.4.3), for comparison with the data from the Munich test-track (Section 2.3.4). The dynamic response to the 5.7 ° loading used in this case was very sensitive to the ballast properties. The velocity FRF normalized by the input force observed at various points in the test-track nevertheless showed good agreement with the experimental measurements (Figure 2.11). The acoustic properties of the 18-sleeper were initially quantified in the frequency range 300–1,500 Hz using the array of virtual measurement points shown, again resulting in satisfactory agreement with experiment, but also certain discrepancies that were attributed to, e.g., acoustic reflections and imprecisions in the far-field to near-field scaling implicit in the calculations. An alternative method was therefore used later for the systematic evaluation of rail pad prototypes (Section 2.4.4).

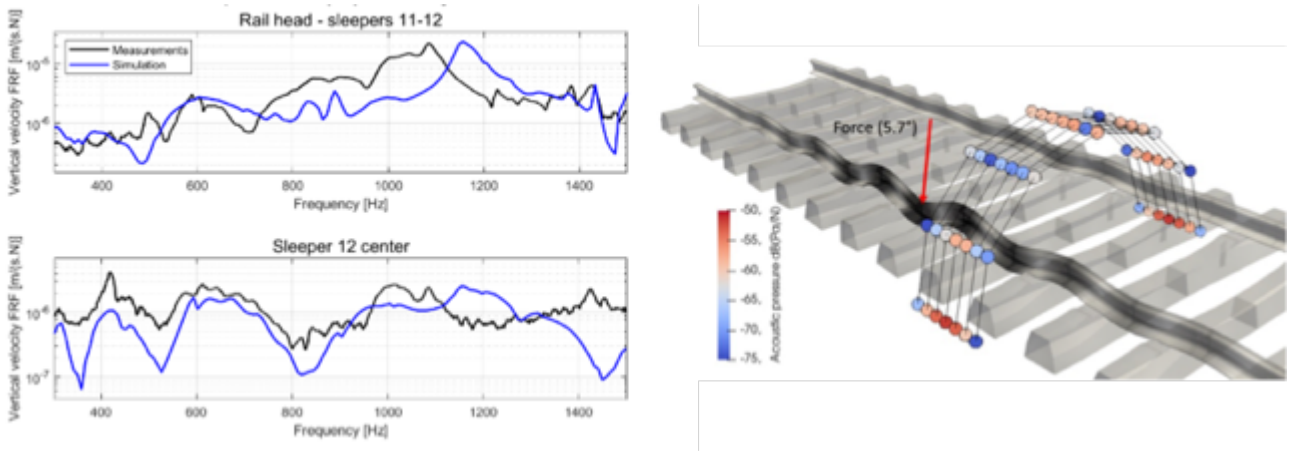

Figure 2.11. Experimental and simulated FRF from points on the excited rail and the 12th sleeper (left) in the 18-sleeper model, shown schematically, together with the virtual measurement points used for the acoustic simulations (right), which correspond to the experimental measurement points. The force was applied to the rail head at 5.7 °, mid-way between sleepers 8 and 9.

2.3.6 Software Implementation for the Public Domain

Improved numerical and semi-analytical full-track modelling tools incorporating the results from the ballast simulations have been implemented and validated. The ensemble of the tools were transferred to freely available open-source software platforms, and provided with user-friendly interfaces and documentation for public release.

2.4 Design, Performance Prediction, Implementation, Testing

2.4.1 Composite Design Approach

Comparative "Ashby diagrams" [34] indicate stiffness and damping to be strongly inversely correlated, the highest damping generally being associated with relatively soft, viscoelastic polymers or related materials, such as bitumen (Figure 2.12). Moreover, if the dynamic moduli, $E'[\omega]$ and $E''[\omega]$, and hence $\tan\delta$, derive from a single relaxation time spectrum through expressions such as Equation 5, it may be shown that [28,29]

$$E''[\omega] \approx \frac{\pi}{2}\left[\frac{\partial E'[\omega]}{\partial \ln \omega}\right]$$

$$\tan\delta[\omega] \approx \frac{\pi}{2}\left[\frac{\partial E'[\omega]}{\partial \ln \omega}\right] \Big/ E'[\omega] \approx \frac{\pi}{2}\left[\frac{\partial \ln E'[\omega]}{\partial \ln \omega}\right] \qquad (7).$$

Close to a dominant transition, where $E'[\omega]$ changes from its low-frequency value, $E'[0]$, to its limiting value at high frequencies, $E'[\infty]$, $\tan\delta[\omega]$ therefore depends on the relaxation strength, $E'[\infty] - E'[0]$, and the width of the transition. $E'[\infty]$ in isotropic polymers is controlled by intramolecular forces and does not exceed a few GPa, but $E'[0]$ may be arbitrarily low unless the polymer is crosslinked, as in PIB, for which $E'[0]$ is of the order of MPa.

Our design strategy implies reducing k' as far as possible for track protection while increasing k'' to reduce noise. In a monolithic polymeric material in uniaxial compression, this amounts to reducing $E'[\omega]$ while increasing $E''[\omega]$. However, Equation 7 shows the maximum in $E''[\omega]$ to coincide roughly with the mid-point of the transition on a log-log scale, fixing $E'[\omega]$ for a given relaxation strength and transition width. These parameters may be manipulated by chemical modification or formulation of existing polymers, so that one may, e.g., centre the frequency of the mid-point of the transition on the frequency range of interest. However, the effective modulus of a soft rail pad may be much higher than E' owing to geometrical constraints, which must be compensated by introducing internal porosity or external profiles (Section 2.3.2), while too low a value of $E'[0]$ may result in rail pads that fail to meet long-term mechanical stability requirements, particularly at high T.

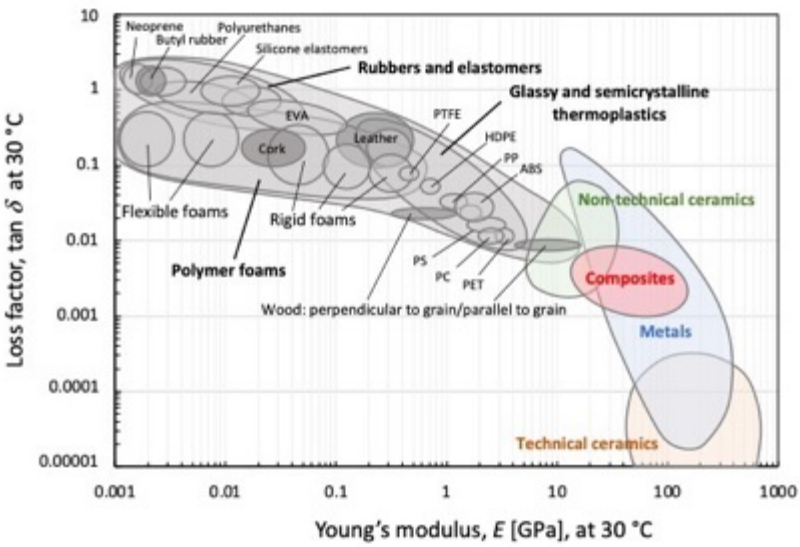

Figure 2.12. "Ashby diagram" of $\tan\delta$ against E at 30 °C for different classes of material [34].

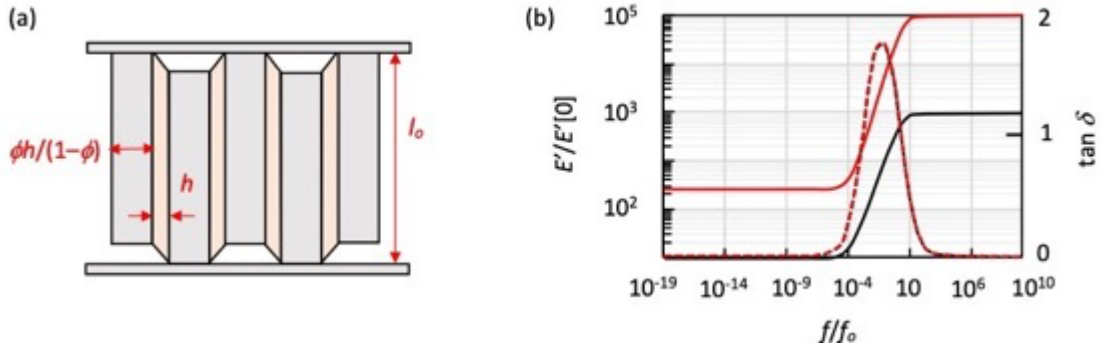

Figure 2.13. Compressive dynamic mechanical response for antiparallel parallelepipedal sheets of thickness h and height l_o of a viscoelastic material, separated by a volume fraction ϕ of infinitely rigid sheets loaded in compression parallel to their planes, *a),* so that the dynamic response is given by Equation 8, shown here for ϕ = 0.2 and l_o/h = 10: the solid and hatched curves designate E and $\tan\delta$ respectively, black for the viscoelastic material and in red for the composite ($\tan\delta$ is identical in the two cases because deformation can only take place in the viscoelastic material).

To provide more design flexibility and better exploit the damping properties of viscoelastic materials, we therefore adopted a composite design strategy based on rail pads that combine hard and/or soft structural components, with high-damping components. A key advantage of this approach is that through a suitable choice of geometry, shear deformation may be concentrated in the high-damping component, while the stiffness may be modulated via the structural component(s). This is illustrated by a geometry (Figure 2.13) in which the high-damping component of an idealized rail pad is in pure shear, resulting in an effective complex modulus for vertical compression

$$E^* \approx \frac{(1-\phi)E_d^*}{3}\left(\frac{l_o}{h}\right)^2 \qquad (8),$$

where ϕ is the rigid phase volume fraction, l_o is the overall thickness, h is the width of the damping layers, and E_d^* is the complex modulus of the damping layers. By making h very small we can make E', and hence k' (there is no lateral constraint on vertical deformation in this case), arbitrarily large, while $\tan\delta$ remains equal to that of damping layers. This requires large deformations in the damping layers and perfect adhesion at the interfaces, and the design is inconsistent with many other practical requirements, but it illustrates how the macroscopic response of a composite may be tailored without the need to modify the chemical structures and formulations of its components *ad hoc*, giving access to a properties that may be impossible to achieve in a monolithic polymeric rail pad. The challenge is then to optimize the

balance between mechanical stability, noise mitigation and superstructure protection, based on feedback from the numerical and analytical simulation tools and laboratory scale tests, taking into account not only the rail pad response in vertical compression, but also deformation modes associated specifically with rail vibrations.

Three types of material representative of the properties we wished to combine in the composite designs were identified for further study at the end of Phase I:

(i) Thermoplastic semicrystalline ethylene vinyl acetate (EVA) as a stiff structural component. EVA is used in the reference SBB hard rail pads provided (glass transition temperature, T_g, of around –10 °C, a broad melting range centred on about 70 °C and $\tan\delta$ of 0.12–0.15 at ambient temperature (21 °C) in the frequency range of interest.

(ii) Porous polyurethane (PU) as a soft structural component. PU may be produced with a wide range of properties and is extremely durable, but serves here as a compressible thermoset elastic phase that may be used for pre-formed inserts, e.g., to replace macroscopic cavities in a composite. It is the base material for soft rail pads currently in use by many rail operators.

(iii) Modified polyisobutylene (PIB) as a high-damping component. PIB is a rubbery copolymer that may be processed as a thermoplastic and crosslinked at 150–200 °C to give the final properties. Commercial high-damping grades of PIB contain large concentrations of carbon black (40 wt%), are lightly crosslinked, and have a T_g in the range –30 to –40 °C, associated with a very strong damping peak centred on about 10'000 Hz at ambient temperature, but which remains strong over a wide frequency range (cf. Figure 2.6). PIB is hence a material of choice in many sound-damping applications. However, commercial high-damping PIB is unsuitable for the production of monolithic rail pads, owing to excessive creep and poor resilience under simulated service conditions.

The resulting materials property palette gave access to a wide range of rail pad stiffnesses, geometrical constraint factors, and damping characteristics. The materials could be combined virtually either in the form of micro-dispersions (blends), or macroscopically, stiffness and stability being provided by an EVA frame, while a PIB laminate core provided damping at acoustic frequencies. A range of two- and three-dimensional (fully encapsulated) core-shell structures with different PIB contents were investigated *in silico* (Section 2.4.3) following the methodology outlined in Section 2.3, and selected designs retained for demonstrator production (Section 2.4.2) and laboratory testing (Section 2.4.4). However, while our initial materials palette was consistent with demonstrator production at the laboratory scale, it was necessary to adapt materials selection as the project progressed for the purposes of up-scaling for the field tests (Section 2.5).

2.4.2 Laboratory-Scale Rail Pad Production

Laboratory production of EVA/PIB demonstrators was carried out in multiple steps using a thermostatically controlled hot press and a mould with modulable inserts, finalized in consultation with a commercial mould manufacturer (Figure 2.14), allowing the PIB content to be varied as required, but with outer dimensions consistent with the specifications provided by SBB (Section 2.1.1). For ease of production we adopted a flat H-shaped geometry rather than the geometry with over-hangs currently used for the hard EVA rail pads, both types of geometry being designed to prevent lateral slip. The modulable inserts were supplemented by disposable hard plastic base-plates produced by fusion deposition moulding ("3D printing") in order to template various profiles to the surface of the rail pad in contact with the rail. All the EVA/PIB demonstrators were produced from rail pad-grade EVA pellets provided by various suppliers, including Semperit, generally containing small amounts of carbon black. The high-damping PIB (Smactane™) was obtained from SMAC SAS, La Garde, France (https://smac-sas.com/en/group/) in an uncrosslinked sheet precursor form that could be cut into the required shape, stacked, and placed in the mould. The EVA pellets were then added, and a press cycle initiated that included a crosslinking step at 150 °C (Table 2.1).

Table 2.1. Typical press cycles for the two types of composite rail pad produced in house.

Composite	Heating step	Heating time [s]	Compression	Compression time [s]	Cooling step
PIB/EVA	120 °C/2 kN	900	150 °C/20 kN	1,800	40 °C/20 kN
SemperSilent™/Hytrel©	160 °C/2 kN	900	190 °C/20 kN	1,800	100 °C/20 kN

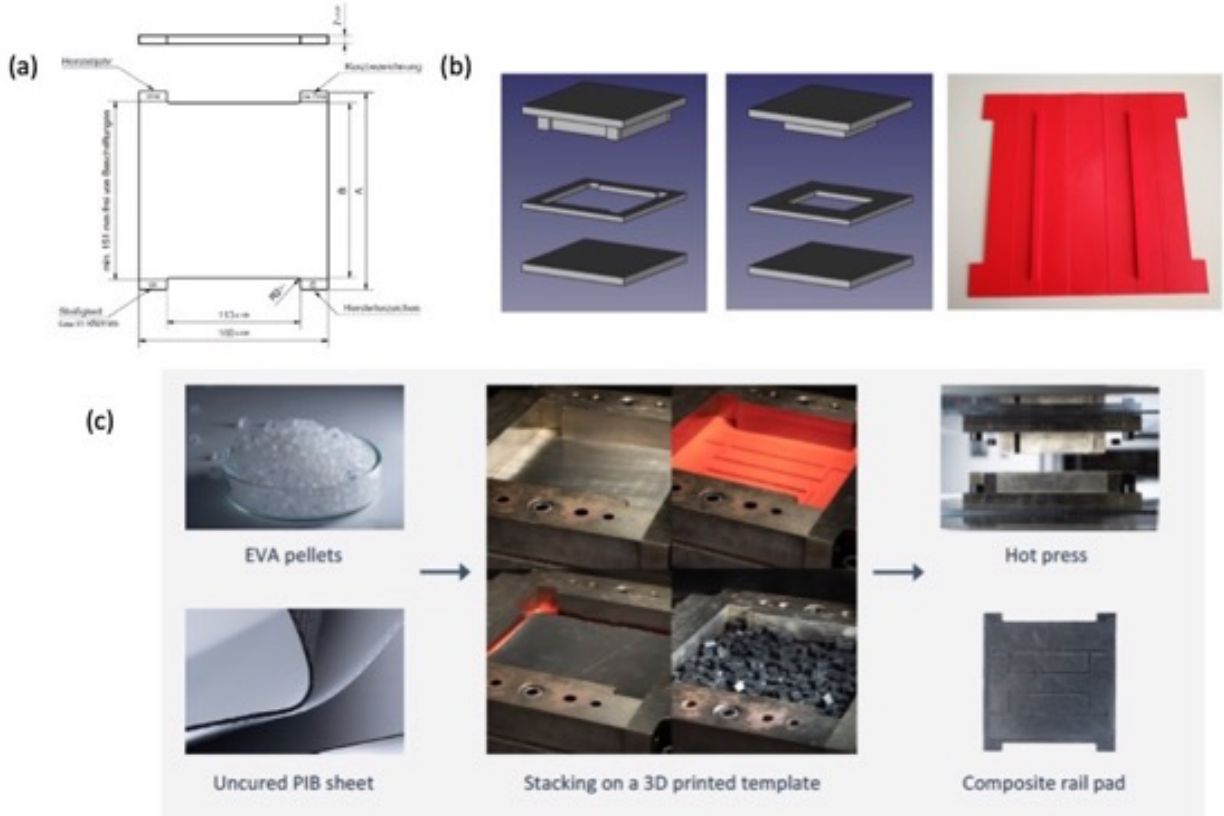

Figure 2.14. Geometry of a mould for *a)* a 7 mm thick H-shaped rail pad, equipped with *b)* a modulable insert for the multi-step production of core-shell composite architectures, together with an example of a three-dimensional printed template for grooved surface profiles (right-hand image). *c)* Photomontage of the processing steps for an EVA/PIB composite rail pad.

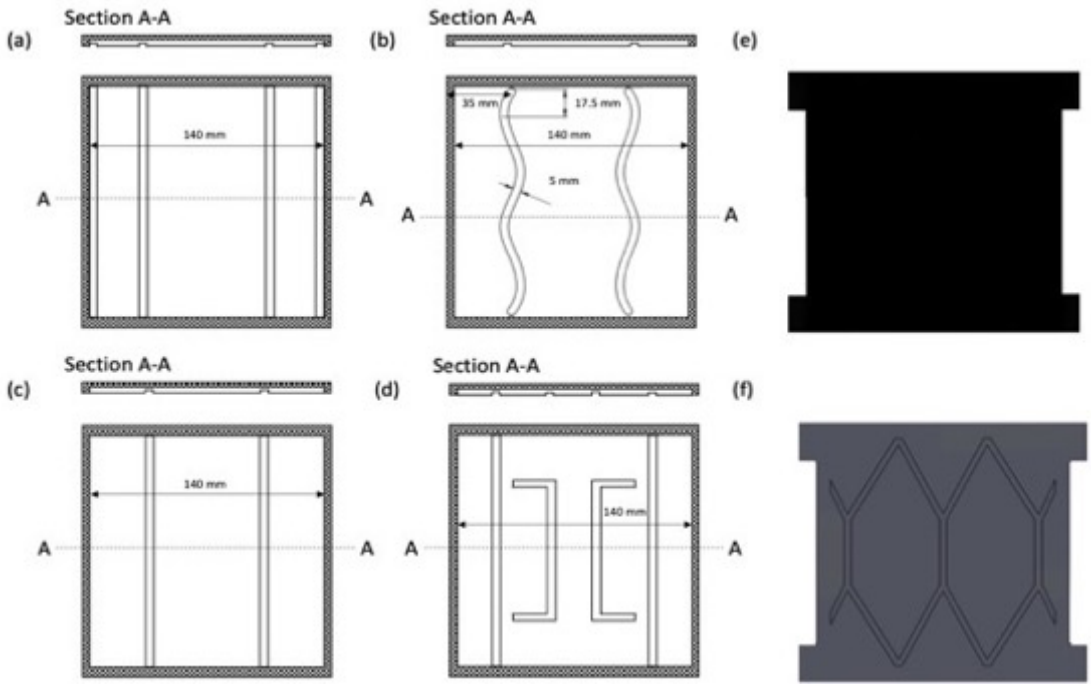

Figure 2.15. Grooved composite rail pad designs retained for standardized testing and further development during Phase II. (Scale drawings of the part of the rail pad under the rail, which was in contact with the grooved face. The shaded regions represent EVA in each case.) *a)* 60 % PIB with four straight surface grooves (k = 477 kN/mm, $\tan\delta$ at 1'000 Hz = 0.63). *b)* 60 % PIB with two undulating surface grooves (k = 472 kN/mm, $\tan\delta$ at 1'000 Hz = 0.72). *c)* 60 % PIB with two straight surface grooves (k = 440 kN/mm, $\tan\delta$ at 1'000 Hz = 0.56). *d)* 60 % PIB with a more complex groove pattern (k = 292 kN/mm, $\tan\delta$ at 1'000 Hz = 0.54). *e)* Actual rail pad produced using a 3D printed template for the grooves, including the overhang to prevent rail pad slippage according to the standard SBB specifications. *f)* Optimized groove design generated by a neural network.

By the end of Phase II, the project was strongly focused profiled rail pads consisting of a single PIB core partially encapsulated by an EVA matrix such that the PIB, which made up approximately 60 % of the rail pad volume beneath the rail, was in direct contact with the rail via a grooved face (Figure 2.15), the grooves being optionally filled with soft, compressible, porous PU, although this had little effect on performance (the principal interest in using PU to fill the grooves was to prevent contamination by dirt or debris in service). Simple configurations were used at first, but later optimization made use of a neural network approach to sample 100'000 randomly generated alternative configurations with respect to k' and $\tan\delta$, estimated using a simplified FE model. Rail pads made from various other materials were also provided by Semperit for assessment during Phase II, based on two profiled geometries designed independently by Semperit prior to their joining the project. Finally, a series of composite rail pads based on a high-damping elastomer, produced by Semperit, referred to for the purposes of this report as "SemperSilent™", and a hard polyester elastomer, Hytrel© 5556 (DuPont de Nemours Inc.), were produced for standardized testing. These materials were chosen to reproduce as far as possible the performance of the EVA/PIB in a configuration in which the high-damping phase could be over-moulded onto the rigid phase, consistent with Semperit processing requirements. One or more Hytrel inserts were first moulded at 210 °C using an aluminium mould and then over-moulded with SemperSilent™ and crosslinked at 190 °C (Table 2.1).

2.4.3 Initial Screening based on Performance Diagrams

We investigated around 100 new rail pad designs during Phases I and II, starting with simple concepts based on analytical and qualitative assessments, followed by refinement according to the simulation results. For initial, coarse screening, we used the semi-analytical model (Section 2.3.4) to predict sound pressures. This model was updated throughout, e.g., with progressively more accurate representations of the ballast (cf. Section 2.3.3). Parametric studies assuming frequency independent rail pad properties nevertheless continued to reproduce the trends identified during Phase I (Section 2.1.4), although, interestingly, a minimum was observed in the noise levels associated with high-damping rail pads at intermediate k' (Figure 2.16a). The average sound pressure, $\bar{p}$, due to rail vibrations between 200 and 2'000 Hz, calculated at a standard virtual measurement point, taking into account the viscoelastic (i.e., frequency-dependent) behaviour of the rail pads, was confirmed to be close to that determined assuming constant and stiffness and damping, represented by k' and $\tan\delta$ determined at 1'000 Hz, the approximate mid-point of this frequency range. This reflected the lack of any marked changes in k' and $\tan\delta$ in the frequency range in question, even in strongly viscoelastic materials such as PIB (Figure 2.6b). Hence, the predicted rail noise for a variety of composite and reference rail pads with various $\tan\delta\,[1{,}000\ \mathrm{Hz}]$ could be combined in a single "master curve" when expressed as a function of $k''[1{,}000\ \mathrm{Hz}]/k_o \approx k''[1{,}000\ \mathrm{Hz}]/k_a$, where k_o was given by Equation 3 with appropriate values of k_a and k_b, depending on the track (Figure 2.16b).

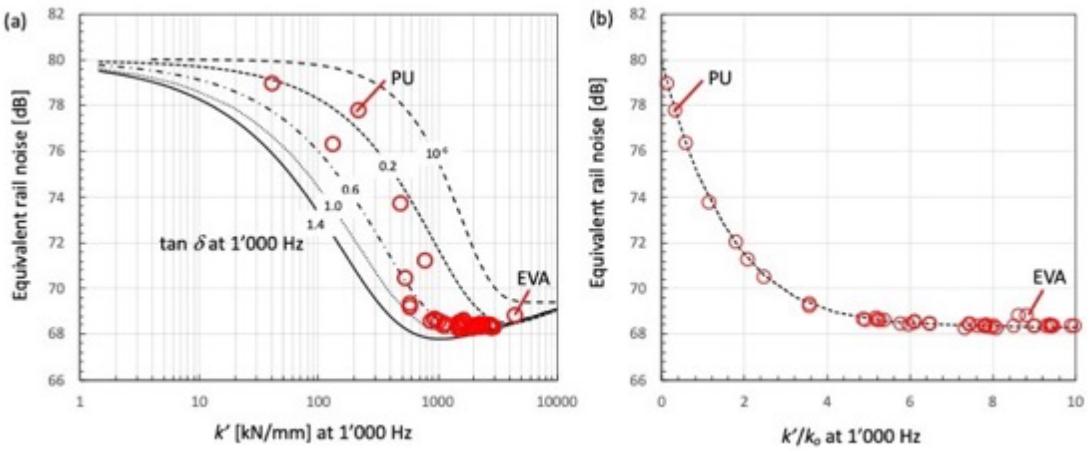

Figure 2.16. *a)* Predicted rail noise levels derived from the average sound pressure between 200 and 2'000 Hz calculated using the semi-analytical model (curves) and plotted as a function of rail pad dynamic stiffness, k', for different $\tan\delta$, assuming frequency independent properties. These results are compared with predictions for various frequency dependent rail pads investigated during Phase II, the reference SBB hard EVA rail pad and a representative soft PU rail pad, plotted as a function of k' determined at 1,000 Hz (circles). *b)* Predictions for the various composite designs plotted as a function of $k'[1{,}000\ \mathrm{Hz}]/k_o$, where k_o is given by Equation 3 (Section 2.1.4) with $k_a = 140$ kN/mm, $k_b = 1'140$ kN/mm and $\tan\delta$ determined at 1'000 Hz.

Correlations such as that in Figure 2.16 facilitated rapid assessment of a given design based on its measured or simulated dynamic properties. For this purpose, data generated by numerical or semi-analytical track simulations, or experimental

measurements were ranked according to simplified indicators for noise and superstructure protection. An *acoustic index*, I_a, was defined as the ratio of the $\bar{p}_{EVA}$, the average sound pressure generated by rails equipped with the reference SBB hard rail pads, to $\bar{p}$ for a given design, so that $I_a > 1$ indicated improved acoustic performance. I_a could conveniently be estimated for high-damping rail pads from a power law fit to the simulated dependence of $\bar{p}$ on k'',

$$I_a = \frac{\bar{p}_{EVA}}{\bar{p}} \approx \left(\frac{k''}{k''_{EVA}}\right)^{\beta} \quad (9),$$

where β was found to be about 1/3 based on the semi-analytical model. A *ballast index*, I_b, was used to characterize track protection, derived from a ballast settlement law from the literature [18]:

$$I_b = \frac{N_{pad}}{N_{EVA}}$$
$$N = exp_{10}\left(\sqrt{S\frac{160}{\sigma}\frac{47}{K_s}} + 2.4\right) \quad (10),$$

where S is a ballast settlement criterion, taken here to be 17.12 mm, N is the number of loading cycles required to reach S for a given maximum compressive stress, σ, in the ballast, and k_s is the ballast stiffness, taken to be 42 MN/m. σ was generally estimated from time-domain pass-by simulations in the three-sleeper cell (typically 160 km/h, 22 ton per axle). $I_b > 1$ hence indicated improved ballast protection, and the observed correlations between I_b, k', and $\tan\delta$ could again be interpolated using a power law. However, while equation 10 is based on rigorous experimental measurements, it is not necessarily representative of the ballast used by SBB and should not be considered to reflect absolute ballast settlement rates in Switzerland. Vibrations remote from the loading point may also contribute to ballast damage. The 18-sleeper model was therefore used to define a second "high frequency" ballast index, I_b^{HF}, from the ratio of the averaged FRFs for the vertical acceleration of successive sleepers along the track, to the value obtained with the reference SBB hard rail pads.

Because the acoustic and ballast indices defined in this way were both positive performance indices, they could be used to establish classical performance diagrams in which simulated or experimental data points corresponding to optimum performance with respect to a benchmark should ideally be clustered in the top right-hand corner of the diagram (Figure 2.17). These performance diagrams provided a rational basis for the selection of rail pads for prototyping, more detailed characterization in the laboratory, and standardized testing with a view to scale-up.

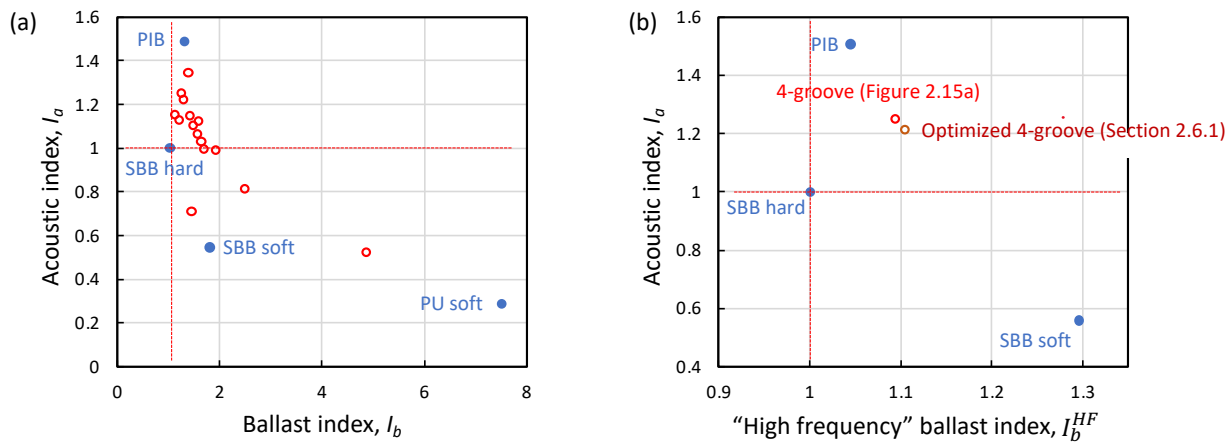

Figure 2.17. *a)* Performance diagram relative to the reference SBB hard rail pad based on numerical/analytical simulations for various composite designs investigated during Phase II, a reference SBB soft rail pad (profiled EVA, Table 2.1), a soft PU rail pad (Table 2.1) and a monolithic PIB rail pad (Table 2.1), where the acoustic index derived from rail noise from the semi-analytical model and the ballast index was calculated from FE simulations of pass-by events using the three-sleeper cell. *b)* Performance diagram for selected rail pads based on the "high frequency" ballast index.

A further important consideration for practical implementation of the new rail pad designs were temperature variations in service. This was not a safety issue, because the limiting low and high temperature properties of the composites were chosen to fall within the bounds represented by existing hard and soft rail pads. However, to investigate the effects on track dynamics we carried out temperature sensitivity analysis on the reference SBB hard rail pads and a representative

high-damping composite rail pad containing 60 % PIB, using both the numerical and numerical analytical models, and assuming extreme service temperatures for Switzerland of –5 and 35 °C. The stiffness of the rail pads increased significantly at –5 °C, as reflected by marked changes in the dynamic response of the model three-sleeper cell, and decreased as T was raised to 35 °C (Figure 2.18). The high-damping rail pad and the reference SBB hard rail pad consequently maintained their acoustic performance at low T, but predicted rail noise levels associated with both types of rail pad increased by up to 3 dB at 35 °C. It was nevertheless concluded that the acoustic performance of high-damping rail pads should continue to exceed that of the reference rail pads over most of the expected range of service temperatures.

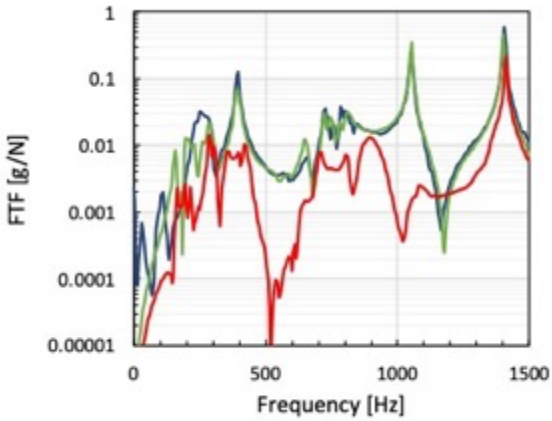

Figure 2.18. Dynamics of the three-sleeper cell fitted with the reference SBB hard rail pads: experimental results at 20 °C (blue), simulation at 20 °C (green) and simulation at -5 °C (red).

2.4.4 Experimental and Numerically Simulated Sound Levels for Selected Rail Pads

Comparison of simulated noise levels with noise levels measured using the three-sleeper cell (Figure 2.19) were well correlated and a strong basis for comparative evaluation using the simulations. However, the simulated values were systematically lower than the measured values for strongly damping rail pads in this set-up, and relatively insensitive to nature of the rail pad profiles, emphasizing the importance of the experimental measurements for detailed assessment. These differences in noise level among the different rail pads were strongly associated with specific resonances and the corresponding frequency sub-bands (Figure 2.20). It could be seen, e.g., that the most promising composite prototypes from Phase II, the 4-groove EVA/PIB composite rail pad (Figure 2.15a) and the D-groove EVA/PIB composite rail pad (Figure 2.15d), strongly attenuated the resonance peaks seen in the reference SBB hard pad, leading not only to lower overall sound levels over a wide range of frequencies, but also a less "modal" response in comparison with the reference SBB hard rail pads. The modal response was hence particularly marked for very soft non-damping rail pads, including some of the materials provided by Semperit for evaluation, resulting in pronounced resonance peaks and a piercing sound that was far more unpleasant than that produced by the high-damping rail pads, whose frequency spectra were flatter.

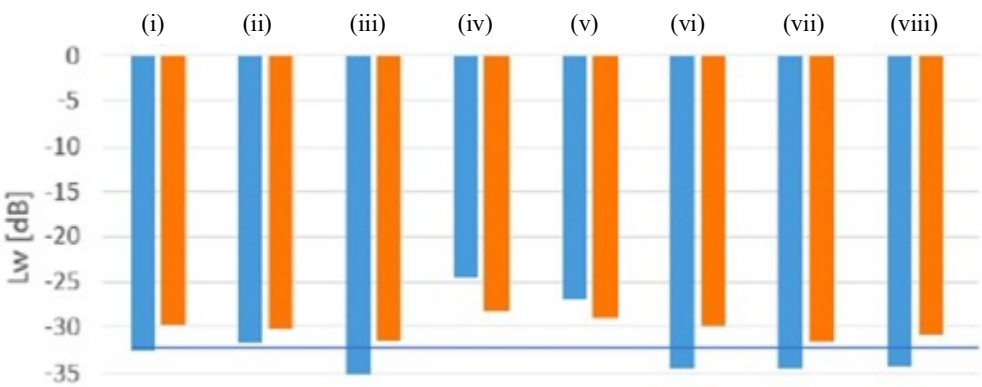

Figure 2.19. Comparison of the simulated (blue) and experimental (orange) normalized logarithmic average sound power levels, L_w, between 300 and 1´500 Hz for an excitation angle of 45 ° for the various rail pads indicated (cf. Table 2.1): (i) reference SBB hard; (ii) reference SBB soft; (iii) monolithic PIB; (iv) PU soft; (v) PU hard; (vi) EVA/60 % PIB composite; (vii) 2-groove EVA/PIB composite (Figure 2.15a); (viii) 4-groove EVA/PIB composite (Figure 2.15c).

The general trends seen with the three-sleeper cell were confirmed by tests on the 4-groove and D-groove EVA/PIB composite rail pads using the instrumented 18-sleeper track section at TU Munich (Section 2.2.4) equipped with a real ballast. Sound pressure levels measured at mid-point of the track under similar shaker excitation conditions indicated both the high-damping rail pads to be 3–5 dB quieter than the reference SBB hard rail pads in the frequency range 1,000–2,500 Hz, with somewhat better overall performance being seen for the 4-groove rail pads (Figure 2.21). These tests also highlighted the potential of the softer high-damping rail pads for improved track protection and suppression of ground

vibrations, as evidenced by the various FRFs between the rails, sleepers, and ballast, and data obtained directly from the vibrometers.

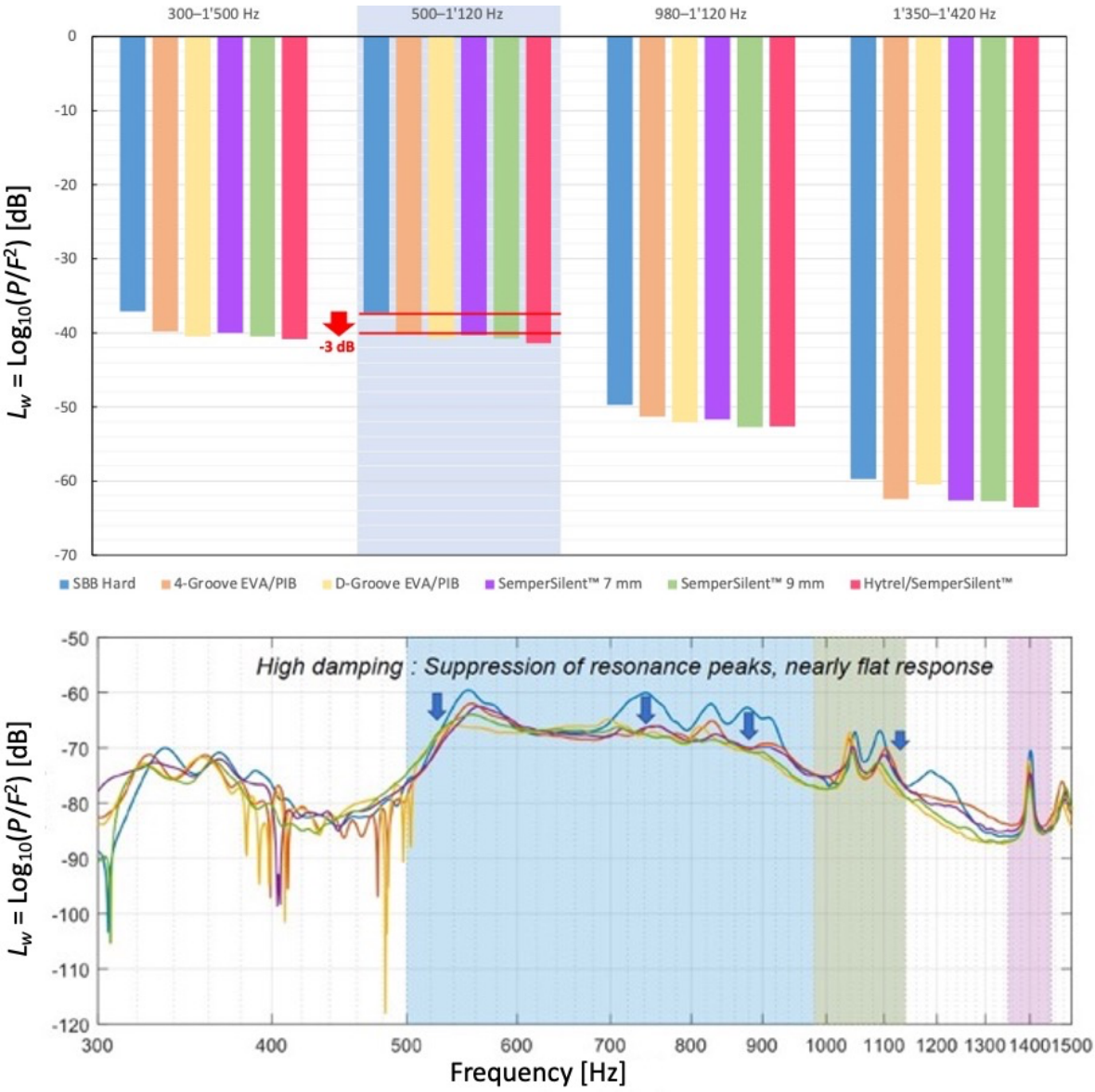

Figure 2.20. Comparison of the normalized logarithmic average sound power levels for an excitation angle of 5.7 ° in different frequency bands from the experimental three-sleeper cell equipped with reference SBB hard rail pads, selected Phase II composite prototypes (4-groove and D-groove EVA/PIB composite rail pads (Figures 2.15a and d, respectively)), the 7 and 9 mm (Table 2.1) thick prototypes provided by Semperit made from the high-damping elastomer SemperSilent™, and the most recent Hytrel/SemperSilent™ composite prototye (Section 2.5.2, Table 2.1) . Corresponding continuous spectra are also shown, illustrating the effect of damping on the resonance peaks. It is seen from these latter that the averages included artifacts in the low frequency regime below 500 Hz which was little influenced by the rail pad properties and is of limited importance for A-weighted noise levels. Moreover, the high frequency resonance at about 1'400 Hz is a consequence of the reduced length of the experimental cell and was absent from full-track simulations. For these reasons, we considered the 500–1'120 Hz frequency band, indicated in blue, to be of most relevance for comparison of the different designs.

Also shown in Figure 2.20 are data from the single material rail pads produced by Semperit at different stages of development and scale-up for field tests (Section 2.5.3), and whose stiffness and damping were comparable those of the best EVA/PIB composite rail pads (Table 2.1). Indeed, the 9 mm thick SemperSilent™ rail pads initially provided by Semperit showed excellent acoustic properties, similar to those obtained with the composite prototypes for both 5.7 ° and 45 ° excitation angles. This could be attributed in part to their greater thickness and the consequent increase in the volume of viscoelastic material that contributed to damping. The acoustic properties of the SemperSilent™ rail pads remained very good when their thickness was reduced to 7 mm, which resulted in a reduction in $\tan\delta$, but also increase in stiffness (Table 2.1), although they were still significantly softer than the composites. However, the best response was

obtained with a Hytrel/SemperSilent™ composite prototype developed during Phase III (Table 2.1), consistent with the exceptional acoustic properties determined *in silico* for this design, which will be discussed in more detail later in this report (Section 2.5.2).

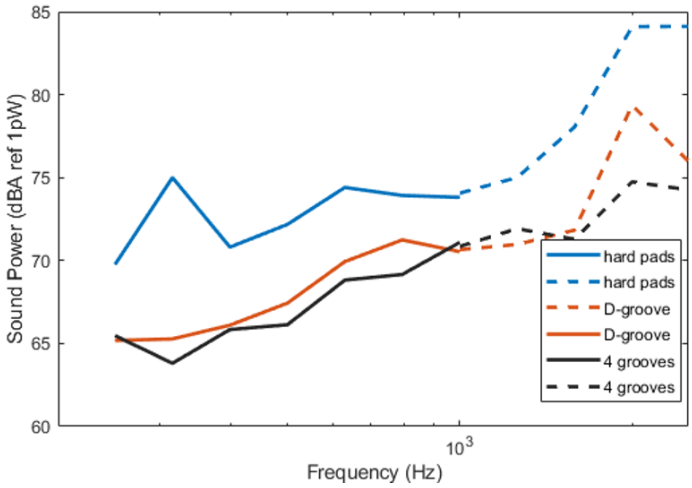

Figure 2.21. Comparison of the logarithmic A-weighted average sound power output for a shaker excitation angle of 5.7 ° measured at a standard measurement point mid-way along the TU Munich test track, equipped with reference SBB hard rail pads, and the 4-groove and D-groove EVA/PIB composite rail pads (Figures 2.15a and d, respectively) as indicated. The full and dashed lines represent two separate frequency sweeps (200–1000 Hz and 900–2'500 Hz).

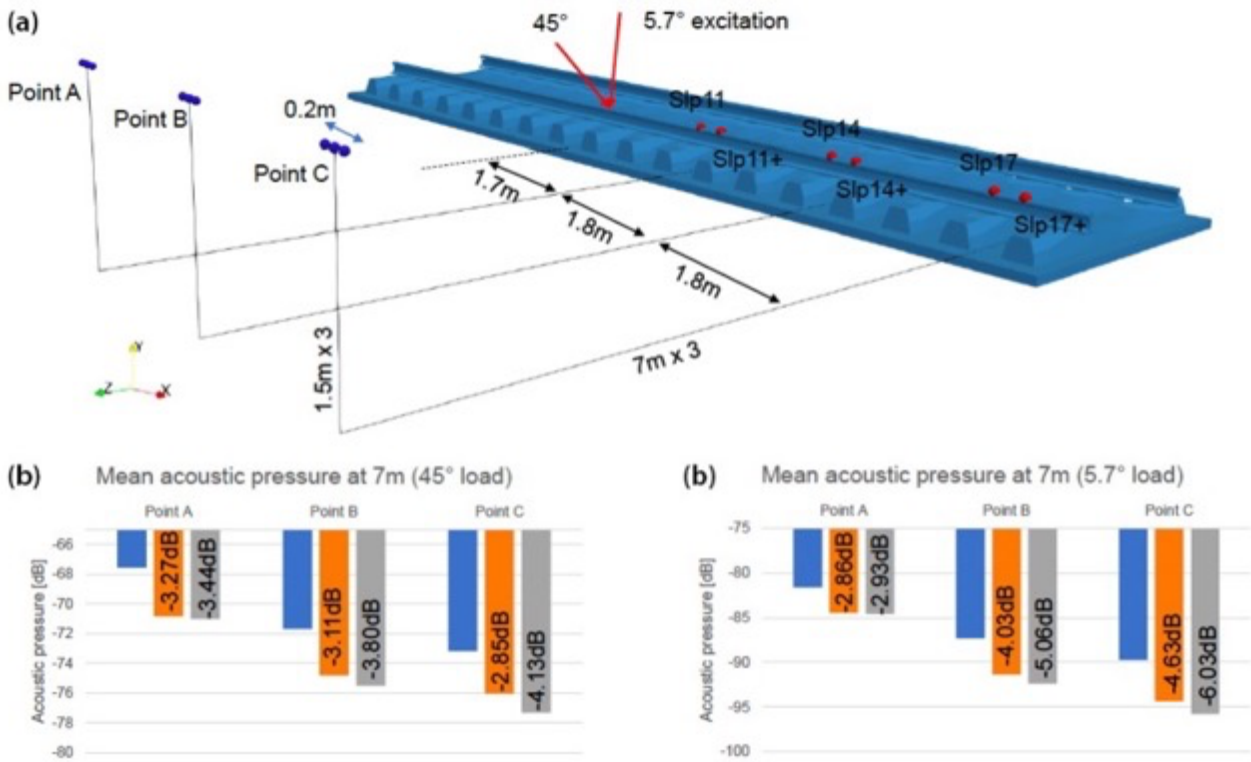

Figure 2.22. Predicted logarithmic average sound pressure for an excitation angle of 5.7 ° at the points indicated in 18-sleeper model equipped with SBB reference hard rail pads (blue), the 4-groove EVA/PIB composite pads (orange) and the 7 mm thick single material prototypes fabricated from the Semperit high-damping polymer SemperSilent™ (grey).

It was not possible to investigate the high-damping single-material rail pads using the Munich test track owing to time constraints, but the availability of the optimized and validated FE simulation tools permitted comparison *in silico* using the 18-sleeper model (Figure 2.22). Acoustic pressure FRFs from the three virtual measurement points shown were averaged to give a mean sound pressure, which was found to be consistent with the acoustic performance of the 7 mm thick SemperSilent™ prototypes in the three-sleeper cell, and also reflected that of the 4-groove EVA/PIB composite rail pads observed in the TU Munich test track (Figure 2.21).

Table 2.2. Summary of the simulated performance indices for the final prototypes described in this section. I_a is the acoustic index defined in Equation 9 calculated from the 18-sleeper for a 5.7 ° excitation (Figure 2.21) and expressed as a logarithmic sound power level relative to that of the reference SBB hard rail pads [dB], I_b is the ballast index defined in Equation 10 and I_b^{HF} is the "high frequency" ballast index calculated from the FRFs for vertical acceleration (Section 2.4.3).

	$20\log_{10} I_a$	I_b	I_b^{HF}
Opt 4-groove EVA/PIB	3.01	1.52	1.10
Hytrel©/SemperSilent™	4.52	1.72	1.34
SemperSilent™ 7 mm	4.32	1.32	1.13

2.5 Final Prototypes and Scale-Up

The final outcome of the composite design loop described in the previous section was a series of composite rail pads that showed excellent acoustic performance under laboratory conditions with controlled excitation, resulting in reductions of 3–5 dB in track noise with respect to the reference SBB rail pads. Of course, neither the simulations nor the experiments reproduced the loading conditions due to a passing train, and no attempt was made to include wheel noise. However, wheel noise is expected to result in a constant background with a significantly lower intensity than track noise [35]. We were therefore confident that the new high-damping rail pads would lead to measurable improvements in sound levels recorded during train pass-by events on a full-scale track, justifying scale-up and organization of field tests in Phase III. Unfortunately, although the final composite prototypes met the various technical requirements (Section 2.5.1), it was not possible to scale up production of this particular combination of materials in time to meet the project deadlines. We therefore opted to carry out the field tests on a high-damping single-material (SemperSilent™) rail pad produced by Semperit, which has already been referred to extensively in previous sections. This again led to promising acoustic properties, as confirmed experimentally at the laboratory scale (Figure 2.20), and could be mass-produced without modification to the Semperit production process (Section 2.5.3). At the same time, we continued to investigate composite designs compatible with the Semperit production process and based on readily available alternatives to EVA and PIB, allowing very rapid generation of an additional final prototype (Section 2.5.2), with exceptional noise and ballast protection properties. The simulated performance indices for the ensemble of the final prototypes are given in Table 2.2, and their properties and standardized testing are described in more detail in the remainder of this section.

2.5.1 First Generation Composite Prototypes (EVA/PIB)

TU Munich was mandated to carry out the standardized stiffness and fatigue tests on what was considered to be the most promising EVA/PIB composite design from Phase II, namely the 4-groove EVA/PIB composite rail pad (Figure 2.14a), i.e., EVA/60 % semi-encapsulated PIB with four straight grooves in contact with the rail, a static vertical compressive stiffness of 477 kN/mm, and $\tan\delta$ of 0.30 and 0.33 measured at room temperature, and 10 and 20 Hz, respectively. TU Munich is a certified institute and was supplied with an SBB sleeper for the fatigue measurements according to EN-13146, i.e., 3,000,000 cycles at 4 Hz on a 33° inclined pad. The results showed significant plastic deformation of the EVA shell, resulting in a loss in stiffness that exceeded 25 %, so that the original design did not meet homologation requirements. Compression tests on the EVA used for the rail pad together with the EVA from the

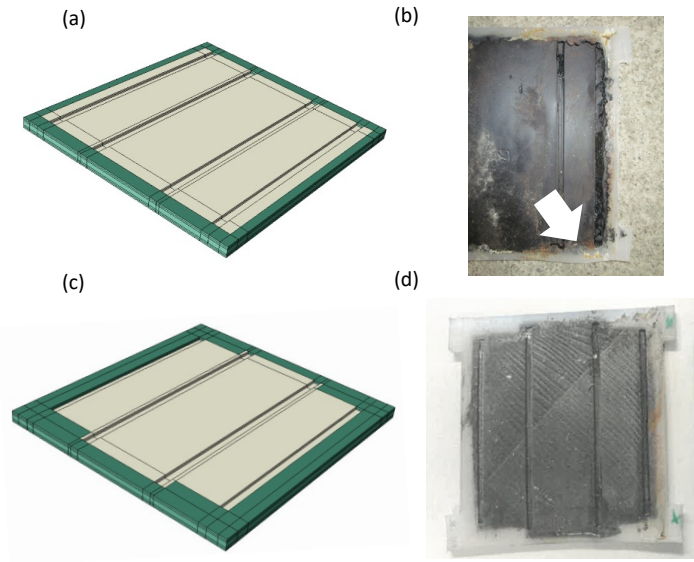

Figure 2.23. Results from fatigue testing at TU Munich according to EN 13146. *a)* Initial geometry of the contact face of the 4-groove EVA/PIB composite pad (green = EVA, grey = PIB). *b)* Plastic deformation of the EVA shell after 3,000,000 cycles (indicated by the arrow). *c)* Initial geometry of the contact face of the optimized 4-groove EVA/PIB composite pad (green = EVA, grey = PIB). *d)* Optimized 4-groove EVA/PIB composite pad showing no plastic deformation after 3,000,000 cycles.

reference SBB hard rail pad, indicated the effective yield stress to be about 20 MPa in the absence of constraints, whereas the compressive stress on the EVA rim of the prototype tested in Munich was estimated from FE simulations to reach 25 MPa for an applied load of 86 kN, the amplitude of the loading cycle used for the fatigue tests.

Optimization, i.e., redesign of the EVA shell to reduce the maximum compressive loads to well below its yield stress (Section 2.3.2), resulted in a static vertical compressive stiffness of 527 kN/mm, and $\tan\delta$ of 0.20 and 0.25 measured at room temperature, and 10 and 20 Hz, respectively. The stiffness and damping therefore remained similar in the two designs, implying similar acoustic and ballast protection performance (cf. Figure 2.17b). Standardized testing according to EN-13146 was repeated at Kunststoff Technik Leoben, a certified partner institute of Semperit. The rail pads in this case met the standard requirements, minimal plastic deformation and stiffness loss being observed after 3,000,000 fatigue cycles, and satisfactory results were also obtained from longitudinal slip tests (Figure 2.23). Full reports for the 4-groove EVA/PIB composite rail pads and the optimized 4-groove EVA/PIB composite rail pads are available on request.

2.5.2 Second Generation Composite Prototypes (Hytrel©/SemperSilent™)

Although time constraints imposed a single-material design for the field tests, development of composite designs continued in collaboration with Semperit with the aim of replacing EVA with a more heat-resistant material to allow over-moulding of either a PIB or a SemperSilent™ core as part of an industrial process. The initial candidate for rigid component was polyamide 6,6, which is already used to manufacture hard rail pads. Prototypes were fabricated at the laboratory scale based on the optimized 4-groove design, but the use of polyamide 6,6 was found to lead to unacceptably high values for the compressive stiffness. It was therefore proposed to replace polyamide 6,6 by a high temperature thermoplastic elastomer from the DuPont Hytrel© range of polyesters, which was combined with SemperSilent™ in various geometries using the hot press (Section 2.4.2). The final design (Figure 2.24) consisted of a grooved SemperSilent™ shell with 2 mm thick grooved Hytrel plates embedded in both surfaces and angled at 90 ° to each other. The intent was to place the high-damping material where most deformation occurred on excitation of the rails according to the simulations, while reinforcing the rail pad elsewhere. These rail pads had a static vertical compressive stiffness of 372 kN/mm, and $\tan\delta$ of 0.16 and 0.25 measured at room temperature, and 10 and 20 Hz, respectively, and are currently undergoing fatigue testing according to EN-13146 at Kunststoff Technik Leoben with a view to scale-up. Their exceptional acoustic performance *in silico* (Table 2.2) reflected the results of laboratory tests using the three-sleeper cell (Figure 2.20).

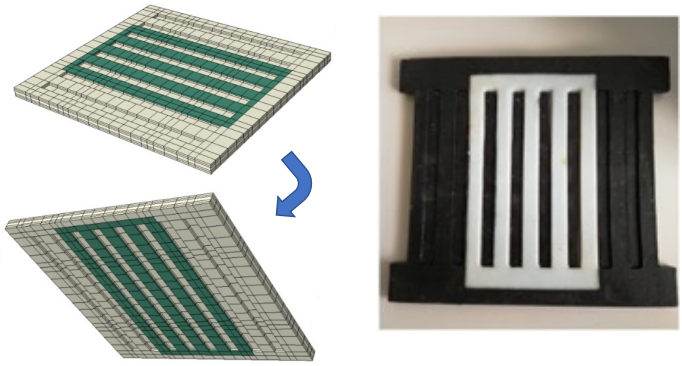

Figure 2.24. Hytrel (white)/ SemperSilent™ (black) composite design: top view showing one of the grooved Hytrel inserts, the other being embedded in the bottom surface at 90 ° to the top plate, as shown schematically (left).

2.5.3 Single-Material Prototypes for Scale-Up and Field Testing (SemperSilent™ 7 mm)

Having established detailed superstructure-related technical requirements for the new rail pads together with SBB, Semperit selected a high-damping material, and a rail pad geometry consistent with the performance targets of the project (stiffness, damping, and fastening system requirements). These were made available to the rest of the consortium for analysis, together with a range of alternative materials, and were found to be of interest for implementation. In order to equip the Nottwil test section with optimized rail pads on schedule, Semperit was then asked to design an optimized rail pad, which we refer to here as the "SemperSilent™ 7 mm" rail pad, and produce an appropriate production mould, which they were able to do at short notice. The modelling toolchain was used extensively in the evaluation and design optimization process, e.g., the single rail pad model (Section 2.3.2) was used to evaluate the static, dynamic stiffness, and damping properties, while the three-sleeper cell model was used to evaluate the vibrational and acoustic properties, and the ballast protection index used in the performance plots (Section 2.4.3). The final rail pads had a static vertical compressive stiffness of 244 kN/mm, and $\tan\delta$ of 0.31 and 0.40 measured at room temperature, and 10 and 20 Hz, respectively. Before installation, the optimized pads were tested according to SBB specifications, and their damping properties were also found to be promising according to results from Semperit's own TDR test bench. After approval by SBB, 400 rail pads were produced, delivered, and installed in the test track at Nottwil in mid-March 2022 (Section 2.2.5).

2.6 Field Tests on Scaled-up Prototypes (Single-Material SemperSilent™ 7 mm, Nottwil)

The results of the field tests carried out at Nottwil (Section 2.2.5, Figure 2.27) are currently undergoing full statistical analysis [36] and will only briefly be summarized here, with emphasis on train pass-by noise measurements, which were of most importance in the light of the design targets. However, tests were also carried out on the track itself, allowing extraction of parameters relating to track mobility and vibration transmission, as well as TDR measurements (Figure 2.27). The TDR increased significantly in the section with the high-damping pads (Figure 2.27), while the point mobility of the rail modes (pin-pin vibrations) decreased. Importantly, the sleeper vibration amplitude also decreased by a factor of 1.5–2 starting at 1,000 Hz, indicating better ballast protection with the high-damping rail pads. The very soft Vossloh rail pads installed nearby led to still lower sleeper vibration amplitudes at most frequencies, but also much lower TDR, and their stiffness was in any case well below the range stipulated in the SBB technical requirements (Section 2.1.1).

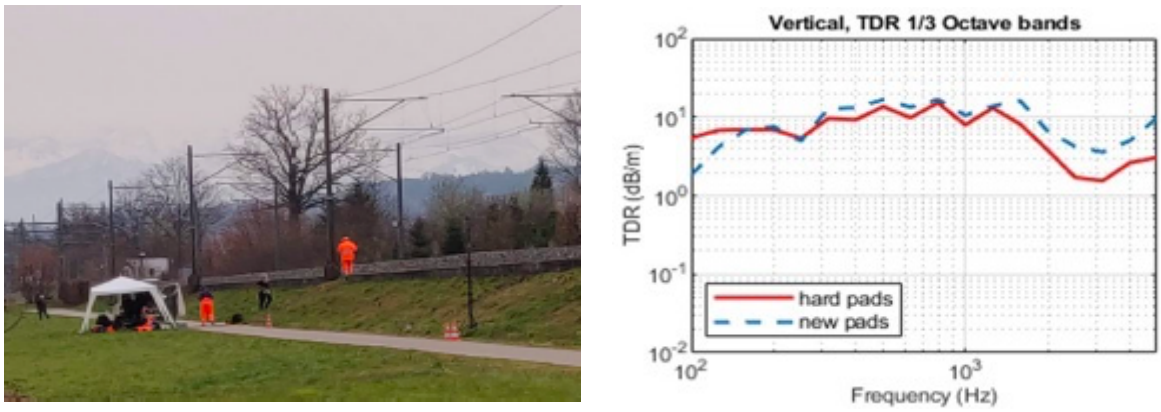

Figure 2.25. Field measurements in progress at Nottwil (left) and results of TDR tests (right) on sections equipped with the reference SBB hard rail pads (A1) and the single material SemperSilent™ 7 mm high-damping rail pads (A2).

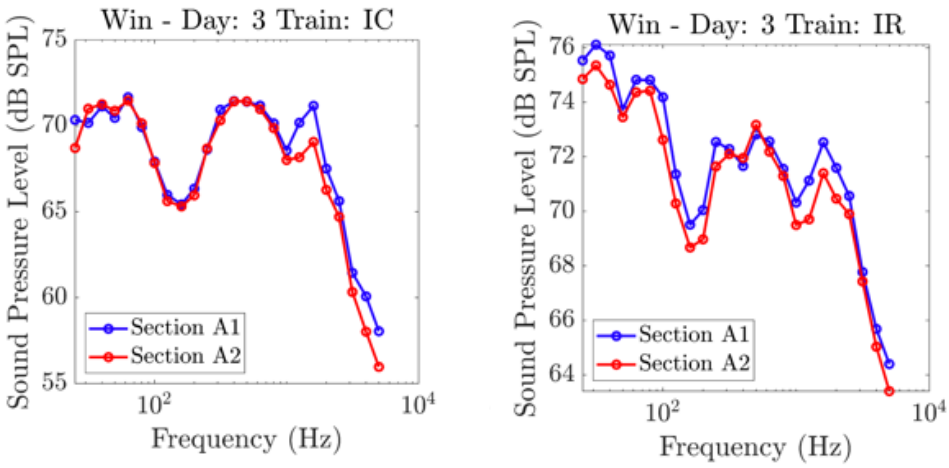

Figure 2.26. Results of sound pressure level measurements for pass-by of Intercity (IC, left) and InterRegio (IR, right) trains on sections equipped with the reference SBB hard rail pads (A1) and the single material SemperSilent™ 7 mm high-damping rail pads (A2), showing significant noise reduction in these latter (microphone position according to ISO 3095:2013, horizontal position 7.5 m from track axis and vertical position 1.2 m above the plane of the railway head).

The pass-by measurements were carried out on three separate days. Day 1 consistent of control measurements prior to installation of the new high-damping rail pads to check that the two sections A1 and A2 gave consistent results with the reference SBB hard rail pads. Days 2 and 3 were then used to compare the high-damping rail pads with the reference rail pads based on 101 pass-by events involving a variety of train and locomotive types and speeds. The different types of train gave significantly different noise signatures, even at comparable speeds. Hence, while the benefits of the of the high-damping rail pads for noise reduction were already apparent when considering results for specific train types (Figure 2.8), in drawing definitive quantitative conclusions from the ensemble of the test results it was important to take into

account the effect of the specificities of each pass-by event, and also to express the results in terms of A-weighted sound pressures, which are of most relevance to the impact of noise on human populations.

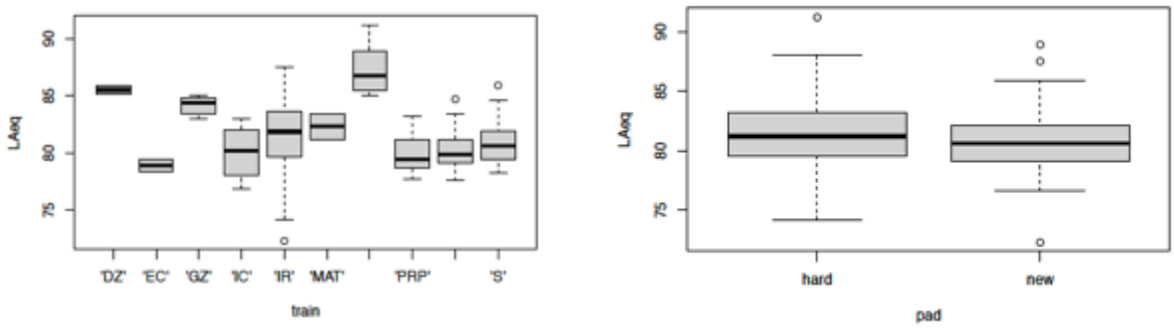

Figure 2.27. The logarithmic noise radiation from 101 trains in normal operation depends on a number of variables, e.g., train type (left), but is reduced by an average of 0.73 dB when the reference SBB hard rail pads are replaced with the SemperSilent™ 7 mm rail pads (right), with high statistical significance ($p < 0.0001$).

In modelling these effects, the A-weighted outcome of the tests, LA_{eq}, was considered as a function of all relevant test variables [36], leading to the statistically significant final result that the mean LA_{eq} decreased by 0.73 dB when the reference SBB hard rail pads were replaced with the SemperSilent™ 7 mm rail pads ($p < 0.0001$ according to Student's t-test). To present this more graphically, we have plotted the LA_{eq} measured for individual trains from the track section with the SemperSilent™ 7 mm rail pads against the values for the same trains from the track section with the SBB hard rail pads (x-axis).

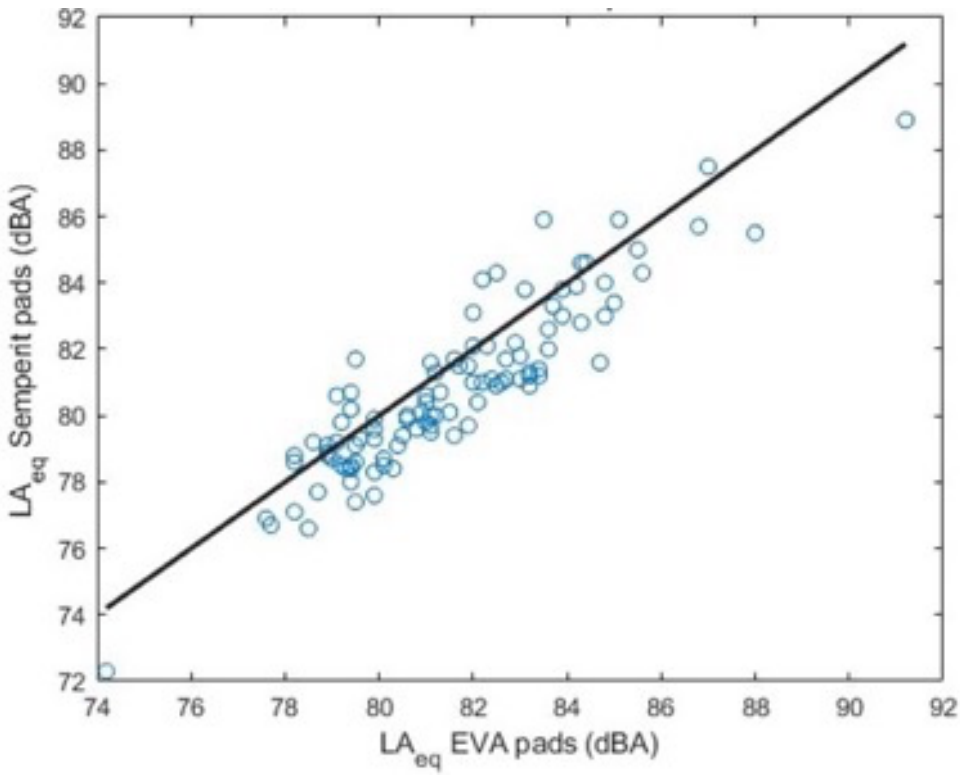

Figure 2.28. LA_{eq} values measured for individual trains from the track section with the SemperSilent™ 7 mm rail pads plotted against values for the same trains from the track section with the SBB hard rail pads (x-axis). Points lying below the curve $x = y$ correspond to a decrease in noise when the reference rail pads are replaced by the high-damping rail pads.

3 Conclusions and Outlook

We successfully brought high-damping rail pad design concepts to fruition through systematic testing and use of validated analytical and numerical simulation tools to extrapolate laboratory-scale measurements to train pass-by on real rail tracks. This was confirmed by field tests, which showed statistically significant reductions in noise for representative Swiss rail traffic by 0.73 dB(A) when reference SBB hard rail pads were replaced by one of the final prototypes that emerged from the work. Moreover, this prototype showed much lower static stiffness than the reference rail pads, implying improved superstructure protection. This was quantified in terms of a ballast index based on an empirical model for sedimentation rates, and sleeper stresses calculated using numerical simulations, supported by field measurements of the stress transfer functions associated with the various track components. It was hence shown that use of the new prototypes should lead to a significant increase in maintenance intervals with respect to those currently employed by SBB for tracks equipped with the reference rail pads. We have hence substantially met the original design targets, namely, a reduction in rail noise by 1 dB(A) with respect to the reference rail pads, a likely increase in track maintenance intervals and hence a decrease in maintenance costs, and compatibility with existing Swiss railway superstructure. As a next step, a concept will be developed by SBB to for the observation of the mid- to long-term behaviour of the new rail pads on a larger scale in several substantially longer track sections and to determine their cost-effectiveness, in terms of both acoustics and maintenance. This information will form the basis for decisions on the future use of the new rail pads.

Our composite approach, which is the subject of a patent application [37], has been key to the achievements of the project, allowing us to modulate rail pad stiffness and damping rapidly by using combinations of well-characterized, readily available rigid and soft high-damping materials, without the need to modify their chemical structure or formulation at each step in the iteration process. The choice of single-material rail pads for the final proof of concept was dictated by practical considerations, e.g., the need to use existing infrastructure for scale-up given the time available for implementation. However, the specifications of these rail pads were carefully designed to match as far as possible those of the final composite prototypes, which were also shown to meet all operational requirements, and have still greater potential, not only for further optimization but also for solutions *à la carte* depending on operators' needs for increased noise reduction, e.g., in built up areas, or increased track protection, e.g., in sections that are difficult to access for maintenance. At the same time, it has become clear that single-valued criteria for noise reduction involving mean sound levels may be insufficient as a measure of the beneficial effects of high-damping rail pads, one of which is to attenuate strong resonances that are perceived to be particularly unpleasant by the listener, and should be considered more systematically in the future when defining what is acceptable in terms of noise.

A further important deliverable has been the modelling tool chain itself, which has enabled us to establish to link materials properties quantitatively to the behaviour of a real track. This has demonstrated, e.g., the value of three-sleeper cell for the experimental characterization of the comparative effect of rail pad properties on track dynamics and noise, despite the rudimentary ballast and limited rail length, implying a more modal response than a large-scale track and the lack of contributions from the TDR. Extrapolation of experimentally validated FE models has shown the effects of rail pad damping to carry over to the multiple-sleeper scale, while the introduction of more realistic representations of the ballast, based on extensive DEM studies, has resulted in quantitatively accurate simulations of the dynamics of a full ballasted track. Parametric investigations based on these latter have in turn allowed us to establish surprisingly simple correlations between the acoustic properties and ballast settlement of a track and the stiffness and damping of the rail pads, indicating that we have come close to absolute limits on what can be achieved in a classical track in terms of noise reduction, but there is still some margin for improvement that we hope will be realized in the near future with the implementation of viable composite designs. Moreover, the impact of the modelling tool chain, which will be freely available to others in the field, is expected to extend well beyond our immediate goal of optimizing rail pad performance, and its development will continue in future projects.

Finally, this project has allowed us to build up significant new core competence, knowledge and insight into rail pads and rail tracks over the past five years that will be invaluable for continued rational development in this area nationally. This has been possible thanks to excellent collaboration between a necessarily diverse group of academic, industrial, and administrative players, each of whom has played a key role in bringing the initial concept from the drawing board to scale-up and implementation, with all the attendant logistical and organizational challenges, many of which were a direct consequence of the measures taken by the Confederation against the ongoing COVID-19 pandemic, as well as sometimes conflicting interests. This has allowed us to make what we hope will be a lasting contribution to the already considerable effort made by SBB to reduce the environmental impact of railways, and develop sustainable solutions for our future transport needs.

4 Acknowledgements

We gratefully acknowledge the financial support of the Swiss Federal Office for the Environment (*Bundesamt für Umwelt*) and the Swiss Federal Office for Transport (*Bundesamt für Verkehr*), and Franz Kuster, Fredy Fischer, Sandro Ferrari, Robert Attinger, *et al.*, for many constructive discussions. Thanks are also due to all who have contributed significantly to the project since its inception (in no particular order): Holger Frauenrath (LMOM-EFPL), Christopher J.G. Plummer (LMOM-EFPL), Oguzhan Oguz (LMOM-EFPL), Alexandre Simula (LMOM-EFPL), Clément Broggi (LMOM-EFPL), Véronique Michaud (LPAC-EFPL), Adrien Demongeot (LPAC-EFPL), Hervé Lissek (LTS2-EFPL), Simone Amorosi (TRACE-EPFL), Joël Cugnoni (COMATEC-HEIG), Maurice Ammann (COMATEC-HEIG), Vincent Crausaz (COMATEC-HEIG), Raphaël Nardin (COMATEC-HEIG), Armin Zemp (Empa), Bart van Damme (Empa), Benjamin Morin (Empa), Balamonica Kalyanasundaram (Empa), Andrea Esposito (Empa), Jakob Oertli (SBB), Urs Schönholzer (SBB).

5 Presentations and Publications

"*Der Einfluss der Zwischenlage auf die Schallemissionen*", Christopher J.G. Plummer *et al.*, Proc. Bahnakustik, Planegg, 15th–16th November 2021, pp 199-208.

"*Nouvelles semelles sous rail pour l'optimisation simultanée du bruit de chemin de fer et de la protection de la superstructure des voies*", Christopher J.G. Plummer *et al.*, CCI France-Suisse, EPFL-TRACE, 17th November 2021.

"*Réduction du bruit ferroviaire*", Holger Frauenrath *et al.*, Federal Office for Transport (OFT), EPFL-TRACE, 7th September 2021.

"Experimental characterisation of the acoustic performance of railway components", Vincent Crausaz *et al.*, Fifth International Conference on Railway Technology: Research, Development and Maintenance, 22nd–25th August 2022, Montpellier, France.

"Railways modelling toolbox: open-source finite element models for rail pads and track optimisation.", Maurice Ammann *et al.*, Fifth International Conference on Railway Technology: Research, Development and Maintenance, 22nd–25th August 2022, Montpellier, France.

"Open source vibro-acoustic finite element modelling of rail tracks components", Raphaël Nardin *et al.*, Fifth International Conference on Railway Technology: Research, Development and Maintenance, 22nd–25th August 2022, Montpellier, France.

"Novel Rail Pads for Improved Noise Reduction and Reduced Track Maintenance", Holger Frauenrath, *Lärmforschung Eisenbahn*, 16th March 2021, Zurich.

"Rail Pad Super-Elements for Track Decay Rate Computation", Benjamin Morin, 13th World Congress in Computational Mechanics, 22nd–27th July 2018, New York, USA.

"Composite rail pad" (Patent EPFL-001-P-CH), Submitted March 2021.

6 Glossary of Symbols and Abbreviations

α	Fitting parameter used to express $\bar{p}$ as a function of k'.
β	Power law exponent used in rough fits of I_a to data for k''.
ϕ	Volume fraction.
ρ	Density [kg/m^3].
σ	von Mises stress [Pa] (representation of the deviatoric components of stress that drive shear deformation).
τ_i	Relaxation times in models for viscoelasticity [s].
ω	Angular frequency ($2\pi f$) [rad/s].
a_T	T-dependent shift factor used for TTS.

BAFU	Swiss Federal Office for the Environment (*Bundesamt für Umwelt*).
CMS	Craig-Bampton modal analysis technique.
dB	Decibel (10 times the ratio of a power quantity to a reference on a logarithmic scale or (equivalently) 20 times the ratio of a root power quantity, e.g., sound pressure to a reference on a logarithmic scale).
dB(A)	Decibel calculated after modifying the sound power by a frequency dependent A-weighting designed to take into account the sensitivity of human ear to different frequencies.
DEM	Discrete element model used for simulation of the mechanics of granular media.
DMA	Dynamic mechanical analysis.
DoF	Degree of freedom of a dynamic system.
E^*	Complex tensile (or compression) modulus [Pa] (equal to $E' + iE''$).
E'	Tensile (or compression) storage modulus [Pa].
E''	Tensile (or compression) loss modulus [Pa].
E_d^*	Complex modulus of a damping layer [Pa].
E_i	Parameters in series expansions for E' and E'' based on a discrete relaxation time spectrum [Pa].
EPFL	Ecole Polytechnique Fédérale de Lausanne.
EVA	Ethylene vinyl acetate copolymer (semicrystalline polymer used to manufacture hard rail pads).
f	Frequency [Hz].
F	Shaker input force amplitude [N]
FE	Finite elements (method for numerical solution of differential equations).
FRF	Frequency response function (acceleration corresponding to unit amplitude excitation force in a dynamic system)
h	Width [m].
HEIG	Haute École d'Ingénierie et de Gestion du Canton de Vaud.
I_a	Acoustic performance index (the ratio of $\bar{p}_{EVA}$ to $\bar{p}$ for a given design).
I_b	Ballast protection index (the value of N that gives the same value of S as for the reference SBB hard rail pads after N = 2'000'000 cycles, normalized by 2'000'000).
I_b^{HF}	"High frequency" ballast index quantifying track vibrations remote from the excitation point.
K	Bulk (hydrostatic compression) modulus [Pa].
k'	Storage stiffness [kN/mm].
k''	Loss stiffness [kN/mm]..
k_a	Fitting parameter [kN/mm] used to express k_o as a function of $\tan\delta$.
k_b	Fitting parameter [kN/mm] used to express k_o as a function of $\tan\delta$.
k''_{EVA}	Loss stiffness of the reference SBB hard rail pads [kN/mm].
k_o	Fitting parameter [kN/mm] used to express $\bar{p}$ as a function of k'.
k_I	Imaginary part of the wavenumber of track vibrations.
k_R	Real part of the wavenumber of track vibrations.
k_s	Ballast stiffness [kN/mm].
LA_{eq}	Average A-weighted sound power level defined in the field tests.

l_o	Thickness [m].
L_w	Normalized logarithmic average sound power levels defined in laboratory tests.
N	Number of loading cycles in a fatigue experiment, number of relaxation times in discrete relaxation time spectra.
p	Sound pressure [Pa].
$\bar{p}$	Average sound pressure [Pa] due to rail vibrations from 200 to 2'000 Hz.
P	Sound power [W].
p_∞	Fitting parameter [Pa] used to express $\bar{p}$ as a function of k'.
$\bar{p}_{EVA}$	Simulated average sound pressure [Pa] generated by rails equipped with the reference SBB hard rail pads.
PIB	Modified polyisobutylene rubber (elastomer commonly used for acoustic damping).
p_o	Fitting parameter [Pa] used to express $\bar{p}$ as a function of k'.
P_{ref}	Reference sound power [W] used in the definition of the sound power level (usually 1 pW).
PU	Polyurethane (class of polymer containing urethane linkages: polyurethane thermoset elastomers are widely used for the production of soft rail pads).
S	Ballast sedimentation [mm]
SBB	Swiss Federal Railways (*Schweizerische Bundesbahnen AG*).
SE	Super-element used to represent the behaviour of the rail pad in semi-analytical simulations.
SemperSilent™	High damping elastomer and corresponding rail pad developed by Semperit.
T	Temperature [°C, K]
$\tan\delta$	Damping ratio, ratio of loss stiffness to storage stiffness (a measure of the rate of energy dissipation per cycle in a dynamically loaded system).
TDR	Track decay rate [dB/m] (measure of the rate of decrease in vibration amplitudes along a track with respect to the excitation source).
T_g	Glass transition temperature [°C, K] (usually associated with strong damping in amorphous polymers).
T_R	Reference temperature used in TTS [°C, K].
TTS	Time-temperature superposition (method for extending the effective frequency range of data for viscoelastic functions at a given temperature using data obtained at other temperatures).
UIC	International Union of Railways.
USP	Under-sleeper pad (elastomeric mat often used to smooth the load distribution at the sleeper-ballast interface).
$10\log_{10}(p/p_{ref})$	Logarithmic representation of a sound pressure with respect to a reference value. ([dB or dB(A)]).
$10\log_{10}(P/P_{ref})$	Logarithmic representation of a sound power (intensity) with respect to a reference value ([dB or dB(A)]). In the standard quantification of noise, P_{ref} is often taken to be 1 pW.
$20\log_{10}(p/p_{ref})$	Logarithmic representation of a sound power with respect to a reference value in terms of the sound pressure ([dB or dB(A)], the power is proportional to the square of the pressure, hence the additional factor of 2 in the pre-multiplier).

7 References

1. Lärmschutzverordnung (LSV) vom 15. Dezember 1986 (Stand am 1. Januar 2016); https://www.admin.ch/opc/en/classified-compilation/19860372/index.html
2. B. Schulte-Werning *et al.* eds., "Noise and Vibration Mitigation for Rail Transportation Systems", Proc 9th International Workshop on Railway Noise, Munich, Germany, 4 - 8 September 2007, Springer (2008); T Maeda *et al.* eds., "Noise and Vibration Mitigation for Rail Transportation Systems", Proc 10th International Workshop on Railway Noise, Nagahama, Japan, 18-22 October 2010, Springer (2011); J Nielsen *et al.* eds., "Noise and Vibration Mitigation for Rail Transportation Systems", Proc. 11th International Workshop on Railway Noise, Uddevalla, Sweden, 9–13 September 2013, Springer (2015).
3. J. Oertli, Erprobung von Schienendämpfern, SBB Schlussbericht, April 2016.
4. J. Oertli, P. Hübner, Railway noise in Europe, A 2010 report on the state of art, UIC, 2010.
5. Schwanen, W., Peeters, B., Lutzeberger, S.: Railway noise in Europe, State of the Art Report, UIC, 2021.
6. https://media.vossloh.com/media/01_product_finder/vfs/system_w_42/Vos_Produktbroschuere_Sys-W42_EN.pdf
7. Kaewunruen, A.M. Remennikov, An alternative rail pad tester for measuring dynamic properties of rail pads under large preloads, Experimental Mechanics 48 (2008), 55–64.
8. J. Oertli, Erprobung von Schienendämpfern, SBB Schlussbericht, April 2016.
9. M. Sol-Sanchez *et al.*, Construction and Building Materials 75 (2015) 293.
10. T.X. Wu and D.J. Thompson, Applied Acoustics 62 (2001) 1249.
11. Milestone Report 1, submitted to BAFU/BAV and the end of Phase I.
12. Stakeholder Analysis (TRACE), submitted to BAFU/BAV and the end of Phase I
13. Milestone Report 2, submitted to BAFU/BAV and the end of Phase I.
14. D.J. Thompson, Railway Noise and Vibration: Mechanisms, Modelling and Means of Control, Elsevier, 2009.
15. D.J. Thompson, P.-E. Gautier, Review of research into wheel/rail rolling noise reduction, Proceedings of the Institute of Mechanical Engineers Part F: Journal of Rail and Rapid Transit 220 (2006), 385-408.
16. A. Kalliainen, P. Kolisoja, A. Nurmikolu, 3D Finite Element Model as a Tool for Analyzing the Structural Behavior of a Railway Track, Advances in Transportation Geotechnics III 143 (2016), 820–827.
17. Railway applications - Noise emission - Characterisation of the dynamic properties of track sections for pass by noise measurements, European Standard EN15461, 2006.
18. N.H.Thom, J. Oakley, Predicting Differential Settlement in a Railway Trackbed. Railway Foundations. Railway Foundations: RailFound 06: 1st International conference on railway foundations: applied research and application to underpin improved railway track design and performance, Birmingham, UK, 11–13 September 2006.
19. C. Jayasuriya, B. Indraratna, T.N. Ngo, Experimental study to examine the role of under sleeper pads for improved performance of ballast under cyclic loading, Transportation Geotechnics 19 (2019), 61–73.
20. R. Insa, P. Salvador, J. Inarejos, A. Roda, Analysis of the influence of under sleeper pads on the railway vehicle/track dynamic interaction in transition zones, Journal of Rail Rapid Transit 226 (2012), 409–420.
21. L. Auersch, S. Said, E. Knothe, W. Ruecker, The dynamic behavior of railway tracks with under sleeper pads, finite-element boundary-element model calculations, laboratory tests and field measurements, Eurodyn 2014: IX International Conference on structural Dynamics, Porto, Portugal, 30 June–2 July 2014, 805–812.
22. N. Vincent, P. Bouvet, D.J. Thompson, P.-E. Gautier, Theoretical optimization of track components to reduce rolling noise, Journal of Sound and Vibration 193 (1996), 161–171.
23. X. Zhang, H. Jeong, D. Thompson, G. Squicciarini, The noise radiated by ballasted and slab tracks, Applied Acoustics, 151 (2019), 193–205.
24. D.J. Thompson, C.J.C. Jones, Noise and vibration from railway vehicles, in S. Iwnicki (Ed.), Handbook of Railway Vehicle Dynamics, Chemical Rubber Company Press, 2006, 279–325.
25. R. Müller, Mitigation measures for open lines against vibration and ground-borne noise: a Swiss overview, Proc. 9th International Workshop on Railway Noise, Munich, Germany, 4–8 September 2007, 264–270.
26. B. Van Damme, A. Zemp, Measuring Dispersion Curves for Bending Waves in Beams: A Comparison of Spatial Fourier Transform and Inhomogeneous Wave Correlation, Acta Acustica united with Acustica 104 (2018) 228–234.
27. UIC project "LOWNOISEPAD", https://uic.org/projects/article/lownoisepad.
28. N. Tschoegl, The Phenomenological Theory of Linear Viscoelastic Behavior, Springer, Berlin, 1989.
29. J. Ferry, Viscoelastic Properties of Polymers 2nd edn., John Wiley & Sons, USA, 1970.
30. H. Schiessel , R. Metzler, A. Blumen, T.F. Nonnenmacher, Generalized viscoelastic models: their fractional equations with solutions, Journal of Physics A: Mathematical and General 28 (1995), 6567–6584.
31. Z.-Q. Qu. Model Order Reduction Techniques: with Applications in Finite Element Analysis. Springer (2004), p. 257
32. P.A. Cundall, O.D.L. Strack, A discrete numerical model for granular assemblies. Géotechnique 29 (1979) 47–65.

33. Oberbau-Simulations-Tool (OST), Abschlussbericht (2015), https://www.aramis.admin.ch/Default?DocumentID=46002&Load=true.
34. M.F. Ashby, Materials Selection in Mechanical Design, 4th edition, Butterworth-Heinemann, UK, 2011.
35. D.J. Thompson, C.J.C. Jones, Noise and vibration from railway vehicles, in S. Iwnicki (Ed.), Handbook of Railway Vehicle Dynamics, Chemical Rubber Company Press, 2006, 279–325.
36. Full field test results are available in the final report by Empa, to be Submitted separately
37. Composite rail pad (EPFL-001-P-CH), Submitted March 2021.